Hydrodynamics of Taylor Flow in Vertical Capillaries: Flow Regimes, Bubble Rise Velocity, Liquid Slug Length, and Pressure Drop

Hui Liu,[†] Chippla O. Vandu, and Rajamani Krishna*

Van't Hoff Institute for Molecular Sciences, University of Amsterdam, Nieuwe Achtergracht 166, 1018 WV Amsterdam, The Netherlands

Two-phase flow hydrodynamics in vertical capillaries of circular and square cross sections were experimentally studied, using air as the gas phase and water, ethanol, or an oil mixture as the liquid phase. The capillary hydraulic diameters ranged from 0.9 mm to 3 mm, with the superficial gas and liquid velocities covering a span of 0.008−1 m/s, which is typical of that obtained in monolith reactors. Using a high-speed video camera, four distinct flow regimes were observed within the range at which experiments were conducted: bubbly, slug-bubbly, Taylor, and churn flows. Annular flow was observed at excessively high gas and low liquid flow rates, well beyond those of interest to this study. Based on the definition of a two-class flow regime, the combination of two parameters—the slip ratio (S) and the ratio of the superficial gas velocity to two-phase superficial velocity (U_G/U_{TP})—was observed to be suitable for determining the transition from homogeneous flow to nonhomogeneous flow. The influence of capillary geometry, capillary hydraulic diameter, and fluid properties on bubble rise velocity (V_b) were investigated and determined to be of little significance. Furthermore, a new and simplified correlation for predicting V_b and, by implication, the gas holdup (ϵ_G) was proposed. Liquid slug lengths were also experimentally studied, using a correlation that was developed to estimate them. Pressure drop experiments were also performed, and the peculiar phenomenon of negative frictional pressure drops was observed at very low liquid velocities. By defining a new dimensionless quantity—the pressure factor, F_E—a flow-regime-dependent method for estimating the total pressure drop in two-phase vertical capillary flows was developed.

1. Introduction

Monolith reactors are becoming increasingly significant as multiphase reactors, considering the advantages that they offer, in comparison to conventionally used trickle beds and slurry bubble columns for a host of processes.[1−5] These advantages, which include low-pressure drop, high gas−liquid mass-transfer rates, and minimum axial dispersion, stem from the uniquely structured multichannel configuration of monoliths. Some studies have shown that the utilization of monolith reactors, in lieu of trickle beds, results in higher productivities and a very significant reduction in reactor size for specified processes.[6,7] Several other studies have focused on the use of monolith reactors for hydrogenation,[8−10] hydrodesulfurization,[11] and oxidation[12,13] reactions, as well as the Fischer−Tropsch synthesis.[14,15]

In essence, a monolith block is composed of an array of uniformly structured parallel channels, often of square or circular geometry, typically having hydraulic diameters between 1 mm and 5 mm. Thus, the monolith can be viewed as a structure that is comprised of many repeating building blocks, where the basic building block is a single channel. It can be argued that data obtained from studies on a single channel, or what may be called a capillary, can be used in scaling up a monolith reactor, provided that a uniform gas and liquid distribution (such as that obtained) occurs in the monolith bundle.[16] Certain multiphase flow characteristics in capillaries have been studied by several investigators, such as gas−liquid flow hydrodynamics,[2,17−20] mass transfer,[2,21−24] and reaction rates.[10,25] These studies were generally performed in the Taylor flow regime, which has been reported to be an effective regime for the operation of monolith reactors. Taylor flow, which is also known as slug flow or bubble train flow, is characterized by the presence of elongated gas bubbles with lengths greater than the capillary diameter, which rise along the capillary separated from each other by liquid slugs. The gas bubbles occupy most of capillary cross section, separated from the channel wall by a thin liquid film. This flow arrangement has been reported to yield superior mass-transfer performance.[17]

Within the past decade, several two-phase capillary studies have focused on one or more of flow regimes, bubble velocity, and pressure drop. Many of these investigations, which involved the use of horizontal capillaries, were limited to air−water systems[26−29] and were geared toward a better understanding of two-phase flow parameters for practical applications in compact heat exchangers, as well as refrigeration and air conditioning systems. Other flow regime, bubble velocity, and pressure drop investigations have involved the use of vertically positioned capillaries.[30−32] Few investigators have used liquids other than water.[2,17,19,33] Taking stock of the various studies that have been undertaken, one observes that limited data are available for capil-

* Author to whom correspondence should be addressed. Fax: + 31 20 5255604. E-mail: R.Krishna@uva.nl.

[†] Permanent address: College of Chemical Engineering, Beijing University of Chemical Technology, Beijing 100029, China.

10.1021/ie049307n CCC: $30.25
Published on Web 12/16/2004

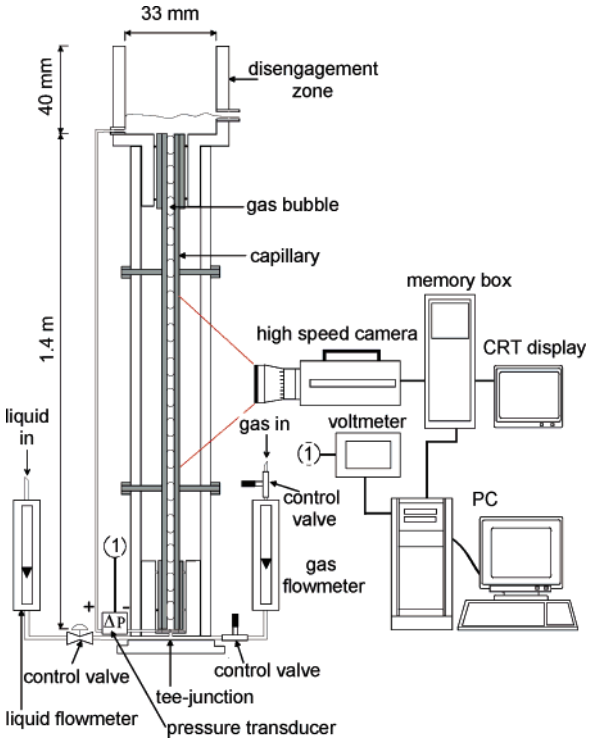

Figure 1. Schematic representation of the experimental setup.

laries of varying geometry and for fluids with surface tension and viscosity values that differ from those of water. The objective of the present investigation is the systematic study of the hydrodynamics of gas−liquid flow in vertical capillaries of circular and square cross sections and the development of correlations for the prediction of related flow parameters such as bubble rise velocity, liquid slug length, and pressure drop. Air was used as the gas phase, with water, ethanol, or an oil mixture being used as the liquid phase. The gas and liquid superficial velocities were varied in the range of 0.008−1 m/s. Within this range, a broad spectrum of flow regimes was encountered. However, particular interest would be focused on the Taylor flow regime, in view of understanding its significance to monolith reactor applications.

2. Experimental Section

A schematic representation of the experimental setup is depicted in Figure 1. It consists of (1) a capillary setup, (2) an image recording and analysis system, and (3) a pressure drop measurement system. The capillary setup is composed of a vertically mounted, 1.4-m-long, single Pyrex glass capillary. Gas and liquid were fed to the bottom of the capillary through a 3-mm-diameter polyvinyl chloride (PVC) tee connection, as shown in Figure 2. Five different capillaries were used in the experiments, and the capillary dimensions and an overview of the experimental systems studied is shown in Table 1. Air was used as the gas phase in all experiments, with the liquid phase being demineralized water, ethanol, or an oil mixture that was a miscible blend of a light paraffin oil (viscosity of $\mu_L = 2.9$ mPa s, surface tension of $\sigma = 28$ mN/m) and a very viscous hydrocarbon oil ($\mu_L = 75$ mPa s, $\sigma = 28$ mN/m) in a volume ratio of 1:2. All experiments were conducted at room temperature and atmospheric pressure. Physical properties of the liquids used are given in Table 2.

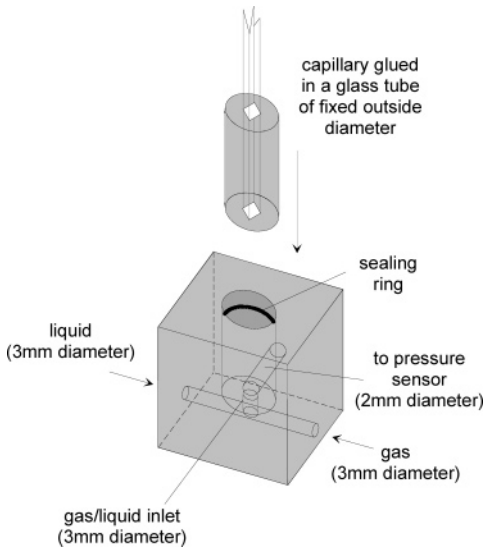

Figure 2. Details of the tee connection.

Table 1. Experimental Systems Studied

gas−liquid system	capillary type	hydraulic diameter (mm)	number of experiments
air−water	circular	0.91	11
air−water	circular	2.00	24
air−water	circular	3.02	44
air−water	square	2.89	39
air−ethanol	circular	0.91	17
air−ethanol	circular	2.00	25
air−ethanol	circular	3.02	17
air−ethanol	square	0.99	27
air−ethanol	square	2.89	41
air−oil mixture	circular	3.02	37
air−oil mixture	square	2.89	24

Table 2. Physical Properties of Liquids Used at 298 K and 100 kPa

liquid phase	density (kg/m^3)	viscosity (mPa s)	surface tension (mN/m)
water	998	0.95	72
ethanol	780	1.2	22
oil mixture	840	15.9	28

Liquid densities were determined using a density meter (PAAR model DMA 35, Austria). Liquid viscosities and surface tensions were measured with a Ubbelohde viscosity meter and by the capillary method, respectively. During experiments, compressed air was fed through a precalibrated float-type gas flowmeter to the tee connection. Two manually operated control valves were used to regulate the gas flow rate. The first of these valves was placed between the compressed air flow line and the flowmeter and was set to give a constant gauge pressure of 30 kPa. The second valve, which was placed between the gas flowmeter and the tee connection, was solely used to regulate the volumetric gas flow rate into the capillary. Liquid was fed from an elevated 10-L storage vessel into a precalibrated liquid flowmeter with the flow rate also adjusted through the use of a manually operated valve. Gravity provided the driving force for the flow of liquid from the storage vessel into the liquid flowmeter. The liquid flowmeter was a float-type flowmeter that had been installed upstream of the tee connection. The gas−liquid flow stream arrangement allowed for an independent alteration of the gas and liquid flow rates. Liquid was discharged from the capillary into a 33-mm-wide, 40-mm-high disengage-

ment zone. The height of liquid in the disengagement zone was ~8 mm.

The image recoding system consists of a Photron model Fastcam-ultima 40K high-speed video camera, a memory box, and a CRT monitor display. The high-speed camera system was used for flow-regime observations and bubble rise velocity measurements. Video movies captured by the high-speed camera were instantaneously stored in the memory box. The camera could be set to capture movies at rates of 30−4500 frames per second (fps) in full-frame mode and 9000−40 500 fps in segmented-frame mode. The CRT display showed, in real time, what was viewed through the high-speed camera. Data from the memory box were transferred to the personal computer (PC) for later analysis. During the experiments, the high-speed camera was positioned midway along the capillary height with its focus adjusted in such a way that it captured rising air bubbles and liquid slugs within a distance of 0.035−0.2 m, depending on the particular operating gas and liquid velocities. After steady state was achieved, movies were made for a certain time span, which varied with bubble velocity, at capture rates of 250−4500 fps, depending on the gas and liquid velocities, to obtain suitable movie time intervals. By performing a frame-by-frame analysis of each movie, the bubble frequency (f_b), which is defined as the number of bubbles that traverse a given point in the capillary per unit time, was determined. The bubble rise velocity (V_b) was also determined from the movies by registering the time required for a gas bubble to rise a known distance along the capillary height. Each V_b value reported is an average of three to five values that were taken. Nevertheless, hardly any of the values differed from the mean value by >4%, indicating that the flow was steady. With the bubble rise velocity known, the gas holdup (ϵ_G) was determined as follows:

$$\epsilon_G = \frac{U_G}{V_b} \tag{1}$$

where U_G is the superficial gas velocity.

In the Taylor flow regime of a vertical upflow capillary, a gas bubble rises along the capillary height sandwiched between liquid slugs. Between the gas bubble and the wall of the capillary is a thin downflowing liquid film. We define a unit cell as consisting of a gas bubble and the accompanying liquid slug beneath it. Furthermore, we assume that, on average, all unit cells have the same length. The average unit cell length (L_{UC}) can then be estimated from

$$L_{UC} = \frac{V_b}{f_b} \tag{2}$$

Assuming that the volume of liquid in the film between the gas bubble and capillary wall is negligible, the average liquid slug length (L_{slug}) can be estimated from the relationship

$$L_{slug} = L_{UC}(1 - \epsilon_G) \tag{3}$$

The pressure drop in the capillary was measured using a differential pressure transducer. Two liquid taps, at the base and top of the capillary, were connected to pressure ports on a Validyne model DP15 pressure transducer, which was, in turn, connected to an analog-to-digital converter card on a PC via a voltmeter (refer to Figure 1). For each liquid used, a calibration curve showing the linear relationship between pressure difference and the voltmeter readings was made. When the capillary was full of a stationary liquid phase, the pressure difference was zero (provided that the same liquid as that used in the capillary also fills the tubes that are connected to the pressure transducer) with a zero voltage reading displayed on the voltmeter as well as being fed to the PC. When only air was present in the capillary, however, pressure difference became equal to the 1.4-m height of the liquid in the tubes that were connected to the pressure transducer. In this case, the span of the voltmeter was set to 10 V. During experiments, pressure drop measurements were performed for a couple of minutes at a sampling frequency of 10 Hz. The experimental system was tested by comparing experimental liquid-only frictional pressure drop data with theoretical frictional pressure drops for laminar flow. For single-phase laminar flow in a vertical capillary, the total pressure drop (ΔP_T) is composed of two contributions: (1) the pressure drop due to frictional effects of the liquid flow (ΔP_f) and (2) the hydrostatic pressure drop of the liquid. Experimental ΔP_f values were obtained by subtracting the hydrostatic contribution from the measured total pressure drop. The theoretical ΔP_f value was computed, noting that, for laminar flow, the Fanning friction factor (f_L) is related to the liquid-phase Reynolds number (Re_L) by the relation

$$f_L = \frac{C}{Re_L} \tag{4}$$

where C is a constant that is dependent on channel geometry and has values of 14.2 and 16 for square and circular channels, respectively. The Fanning friction factor is related to the frictional pressure drop by the relation

$$f_L = \frac{\Delta P_f / L_c}{{}^1/_2 \rho_L U_L^2 (4/d_c)} \tag{5}$$

where d_c and L_c are the diameter and length of the capillary, U_L is the superficial liquid velocity, and ρ_L is the liquid density. Figure 3 shows the experimental single-phase frictional pressure drop with predictions obtained using the f_L values for laminar flow. A very good agreement is obtained, verifying the accuracy of the setup and also helping to ascertain that inlet and outlet effects are negligible.

All the measured experimental data for 11 different campaigns with varying system properties and capillary sizes, and configuration, have been tabulated and presented in the Supporting Information accompanying this publication.

3. Results and Discussion

3.1. Two-Phase Flow Regimes. Typical images of flow regimes observed during experiments are shown in Figure 4 for air−water, air−ethanol, and air−oil mixture systems in the 3.02-mm-diameter circular capillary. A total of five distinct flow patterns were observed and are labeled bubbly flow, Taylor flow, slug-bubbly flow, churn flow, and annular flow. A basic description of each flow regime follows.

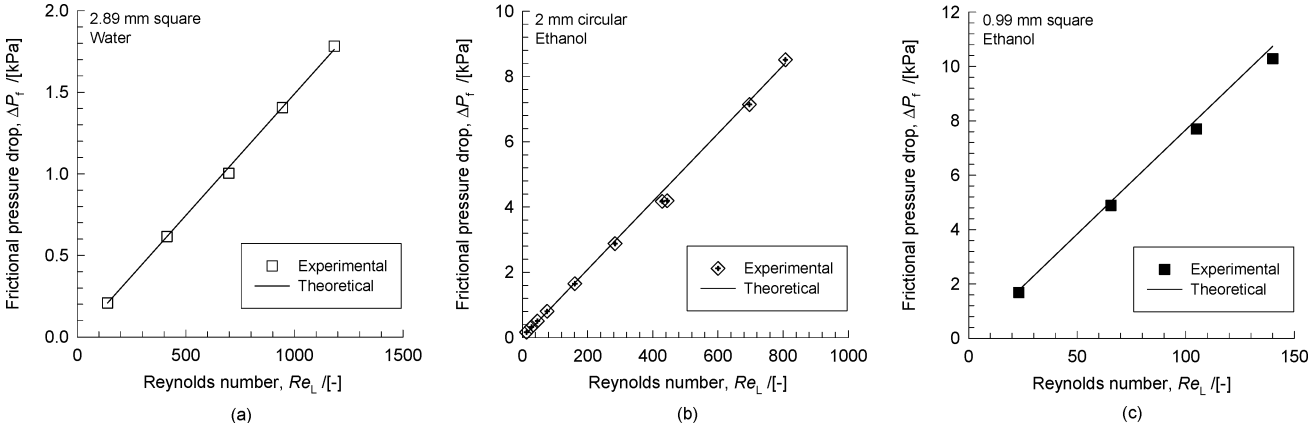

Figure 3. Experimental and theoretical single-phase frictional pressure drop for the (a) 2.89-mm square capillary (water), (b) 2-mm circular capillary (ethanol), and (c) 0.99-mm square capillary (ethanol).

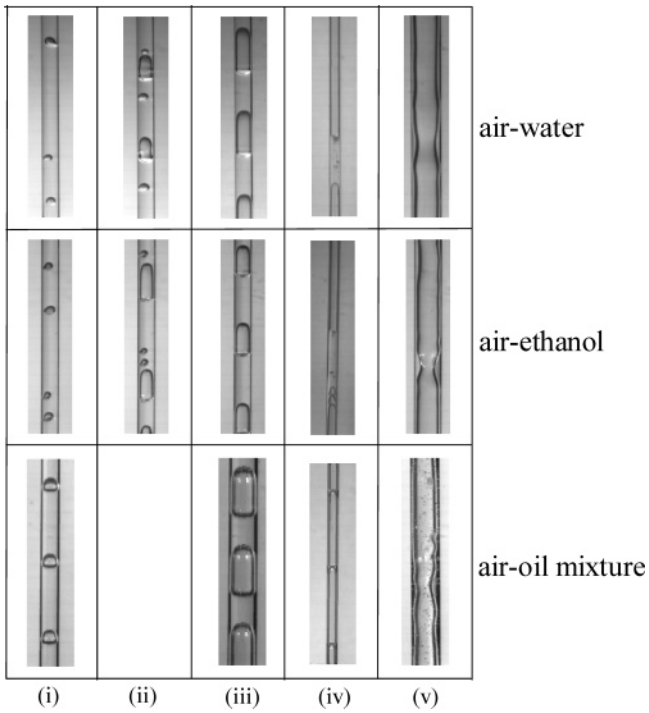

Figure 4. Flow regimes encountered during the experiments performed for air−water, air−ethanol, and air−oil mixtures. Regimes shown are (i) bubbly, (ii) slug-bubbly, (iii) Taylor, (iv) churn, and (v) annular flow. High-speed video recordings of the various flow regimes can be viewed on our website.[35]

Bubbly Flow Regime: This flow pattern typically occurs at relatively high liquid velocities and low gas velocities. It is characterized by the presence of fast rising bubbles with diameters less than or equal to the capillary diameter. The bubbles are often spherical or spheroidal in shape. Gas holdups are generally very low in this regime.

Taylor Flow Regime: Also known as slug flow or bubble train flow, Taylor flow consists of gas bubbles with lengths greater than the tube diameter that move along the capillary separated from each other by liquid slugs. Depending on the gas and liquid flow rates and properties, the bubbles often have hemispherically shaped tops and flattened tails.

Slug-Bubbly Flow Regime: This is a transition regime that occurs between bubbly and Taylor flows. Similar to that observed in Taylor flow, bubble slugs are present, separated from each other by liquid slugs. However, in the slug-bubbly regime, small bubbles are also present in the liquid slugs; this is a feature that is not observed in Taylor flow. The transition from Taylor flow to slug-bubbly flow occurs by increasing the liquid flow rate with the gas flow rate being kept constant.

Churn Flow Regime: Churn flow occurs at very high gas velocities. It consists of very long gas bubbles and relatively small liquid slugs. Because of the high gas velocity, a wave or ripple motion is often observed at the bubble tail with tiny gas bubbles entrained in the liquid slug. Further increases in the gas flow rate result in annular flow.

Annular Flow Regime: At excessively high gas velocities and very low liquid velocities, annular flow results. Here, a continuous gas phase is present in the central core of the capillary with the liquid phase being displaced to form an annulus between the capillary wall and the gas phase.

These flow regimes are what may be called "clear-cut" regimes, because they are easily identifiable. Other investigators have also observed somewhat similar patterns in vertical and horizontal capillaries.[26,30,32,34] A degree of complexity becomes involved when identifying flow patterns that fail to fall into any of the typical regimes depicted in Figure 4. Such patterns can be expected to occur when transitioning from one regime to another, and, in such cases, the discretion of the investigator is heavily relied upon. The slug-bubbly flow regime was not observed for the viscous oil mixture used in this study. Annular flow was not encountered within the range of gas and liquid superficial velocities for which experimental data are presented. Also, all experimental liquid slug lengths reported in this work are for the Taylor flow regime. Movies of the flow regimes depicted in Figure 4 can be viewed on our website.[35]

The flow regime map for the 3.02-mm-diameter circular capillary air−water system obtained from the experiments that have been performed is shown in Figure 5, with the superficial gas and superficial liquid velocities as the x- and y-axes. Furthermore, comparisons are made with some flow regime maps available in the literature. Zhao and Bi[32] studied flow regimes in vertical triangular capillaries for co-current upward air−water two-phase flow. Their experimental data for a 2.886-mm hydraulic diameter capillary is presented for comparison of the bubbly-slug and slug-churn transitions. As can be seen, the slug-churn transition occurs at very close superficial gas and liquid velocities in both capillaries. However, a significant difference exists in

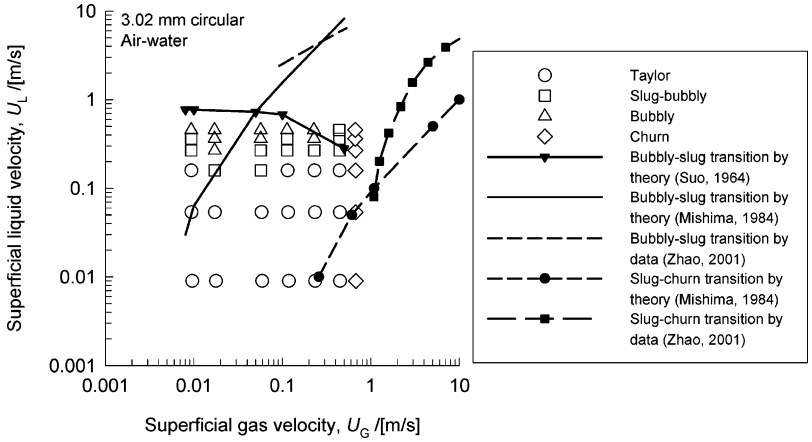

Figure 5. Flow-regime map for the 3.02-mm circular capillary air−water system.

the bubbly-slug transition, a discrepancy that could largely be due to the different gas−liquid distributors used. Although a tee gas−liquid inlet was used in this study, they used a fine-plastic-packed porous mixer to ensure that gas and liquid were well-mixed before entering the capillary. Correlations provided by Mishima and Ishii[36] for predicting flow-regime transitions for upward two-phase flow in vertical capillaries are also compared with our experimental data in Figure 5. Neither the bubbly-slug transition nor slug-churn transition correlations predict our experimental data satisfactorily, with the former showing much larger deviation. Interestingly, they also found that, although these correlations predicted the experimental data of a few investigators, they were not suitable at all for predicting the experimental data of other investigators, partially attributing this to different methods of observations and definitions of flow regimes as well as the fact that transition phenomena develop gradually. The bubbly-slug transition line, based on the correlation of Suo[37] from studies in a horizontally positioned capillary for air−water flow, is also depicted in Figure 5. It qualitatively predicts the trend for transition from the bubbly to slug (Taylor) flow regime.

3.2. Gas Holdup and Bubble Rise Velocity. 3.2.1. Variation of Gas Holdup and Bubble Rise Velocity. The variation of gas holdup ϵ_G with superficial gas velocity U_G for varying superficial liquid velocities U_L is shown in Figure 6a for the 2.89-mm square-capillary air-ethanol system. An increase in ϵ_G results from an increase in U_G and a decrease in U_L. At lower values of U_L, local maximums in ϵ_G are observed. This behavior is often observed in bubble columns and is generally associated with a flow regime transition. A parameter that is often used in two-phase flow analysis—called the slip ratio, S—helps to provide some insight into the relationship between the observed trends in ϵ_G and flow regime transition. The slip ratio S, which is defined as

$$S = \frac{V_b}{V_L} = \frac{U_G/\epsilon_G}{U_L/(1-\epsilon_G)} \tag{6}$$

is a measure of the relative velocity between the gas and liquid phases (where V_L is the liquid-phase velocity). At this point, we can speak of two main classes of flow: homogeneous and nonhomogeneous. Based on the five different flow regimes previously discussed, it can be expected that bubbly flows are typically homogeneous, because discrete gas bubbles are entrained in a continuous liquid phase, which, provided that the liquid velocity is not too high, maintains a Hagen−Poiseuille flow pattern. On the other hand, Taylor, churn, and annular flows are generally nonhomogeneous, with slug-bubbly flow bordering the homogeneous and nonhomogeneous regimes. From eq 6, we note that, if $S \approx 1$, homogeneous flow is obtained, because, under this condition, $V_b \approx V_L$, which is a situation that can only occur when gas and liquid rise uniformly in the capillary with no down flow of the liquid phase. When $S > 1$, bubbles rise with higher velocities than the liquid phase. This can be expected when down flow of the liquid phase occurs in the liquid film surrounding the bubbles, such as that observed in the Taylor and churn flow regimes. In a nutshell, S can serve as an indication of when a two-phase flow deviates from the homogeneous flow regime. To buttress this point, Figure 6a was re-plotted using U_G/U_{TP} and ϵ_G as coordinates in Figure 6b and U_G/U_{TP} and S as coordinates in Figure 6c. U_{TP} is the two-phase superficial velocity, which is defined as

$$U_{TP} = U_G + U_L \tag{7}$$

From these plots, it is seen that, for $U_L = 0.012$ m/s and $U_L = 0.043$ m/s, both of which belong to the Taylor flow regime, deviation from homogeneous flow is most significant, judging by the great increase in S. At higher liquid velocities, the flows gradually approach homogeneous flow, with S values approaching unity. Another characteristic of the large deviation from homogeneous flow is that it occurs at high gas holdups ($\epsilon_G > 0.5$), as observed from a comparison of Figure 6b and 6c. For $\epsilon_G = 0.1-0.5$, the mean S value is ~1.4. Also, the local maximums in ϵ_G shown in Figure 6a can be attributed to the significant increase in slip between phases. In Figure 6d, the flow regime map for the system is shown; lines that correspond to U_G/U_{TP} values of 0.2, 0.5, and 0.8 also are depicted. From this map, it is clear that the increase in S occurs near the churn flow regime and in the Taylor flow regime. The high S operation is predominantly in the Taylor flow regime, whereas a constant S value is observed for the bubbly and slug-bubbly flow regimes.

Plots of the two-phase superficial velocity versus the bubble rise velocity are shown in Figure 7, to demonstrate the effect of certain operating parameters and conditions on the bubble rise velocity. Figure 7a shows that a linear dependence exists between U_{TP} and V_b. Moreover, although V_b shows a strong dependence on U_{TP} (i.e., the combined gas and liquid superficial veloci-

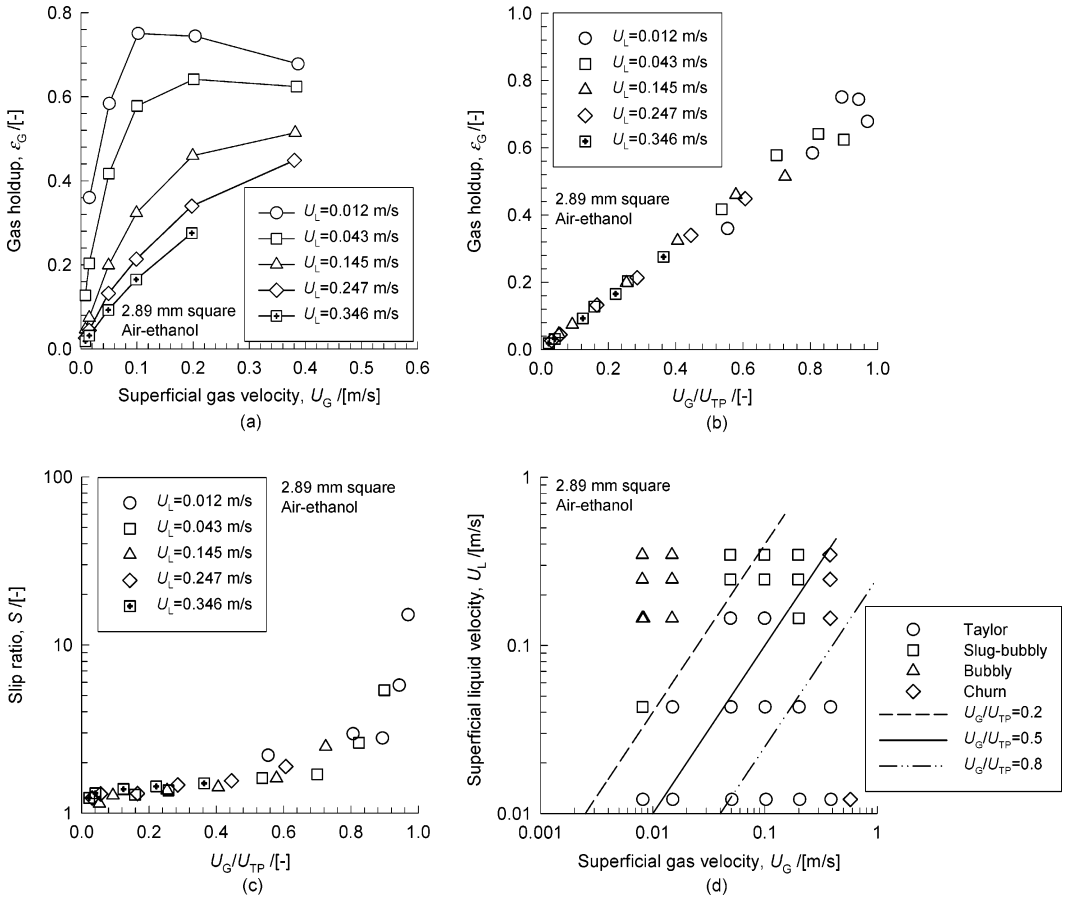

Figure 6. (a) Variation of gas holdup (ϵ_G) with superficial gas velocity (U_G) and superficial liquid velocity (U_L) in the 2.89-mm square capillary air−ethanol system. (b) U_G/U_{TP} versus ϵ_G for the 2.89-mm square capillary air−ethanol system at different liquid velocities. (c) Variation of the slip ratio (S) with U_G/U_{TP} for the 2.89-mm square capillary air−ethanol system at different liquid velocities. (d) Flow-regime map for the 2.89-mm square capillary air−ethanol system.

ties), it shows no dependence on the individual gas and liquid superficial velocities. The effect of capillary geometry on bubble rise velocity is shown in Figure 7b, using air−water data for the 2.89-mm square and 3.02-mm circular capillaries. All data points seem to collapse to a single line, indicating the negligible effect of capillary geometry on bubble rise velocity. Data from the 0.91-mm and 3.02-mm circular capillaries for the air−ethanol system are plotted in Figure 7c, to understand the effect of capillary scale on bubble rise velocity. From this plot, bubbles seem to rise more slowly in the smaller-diameter capillary. This is likely due to an increase in surface tension effect with a decrease in capillary size. In Figure 7d, the effect of liquid viscosity on bubble rise velocity is explored using data from the 3.02-mm circular capillary for air−ethanol and air−oil mixture systems. The oil mixture has a viscosity that is 13 times greater than that of ethanol, whereas the two liquids have similar surface tension values (refer to Table 2). The higher the liquid viscosity, the higher the bubble rise velocity for the same U_{TP}. A similar result was reported by Kreutzer[2] for a 2.3-mm-diameter circular capillary with air and tetradecane as the gas and liquid phases. Tetradecane has a viscosity that is 3 times greater than that of water. The effect of surface tension is depicted in Figure 7e for air−ethanol and air−water systems in the 2-mm-diameter circular capillary. Ethanol has a surface tension that is approximately a third of that for water, whereas both liquids have approximately the same viscosity (refer to Table 2). This plot shows that the surface tension effect only seems noticeable for $U_{TP} > 0.6$ m/s, where the higher surface tension liquid results in a lower bubble rise velocity, although this effect seems to be only slightly pronounced.

3.2.2. Correlating the Taylor Bubble Rise Velocity. Many approaches have been proposed in the literature for estimating bubble rise velocities in a capillary tube. One of these, which is similar to the drift flux model used for studies in larger channels, involves relating the bubble rise velocity to the two-phase superficial velocity:[30,38]

$$V_b = C_1 U_{TP}^{C_2} \tag{8}$$

where C_1 and C_2 are arbitrary constants. However, these arbitrary constants are dependent on such parameters as the tube diameter and liquid properties, serving as a drawback to this method. Another method for estimating the bubble rise velocity involves conducting a mass balance about a unit cell for a fully developed steady Taylor flow, resulting in the relationship

$$\epsilon_{Lf}(V_b - V_f) = V_b - U_{TP} \tag{9}$$

where ϵ_{Lf} and V_f are the liquid film holdup and liquid film velocity, respectively. Based on the works of Thulasidas et al.[17] and Barnea,[39] independent estimations of ϵ_{Lf} and V_f can be made from which the bubble rise velocity can, in turn, be determined. However, this approach is cumbersome, because it requires that

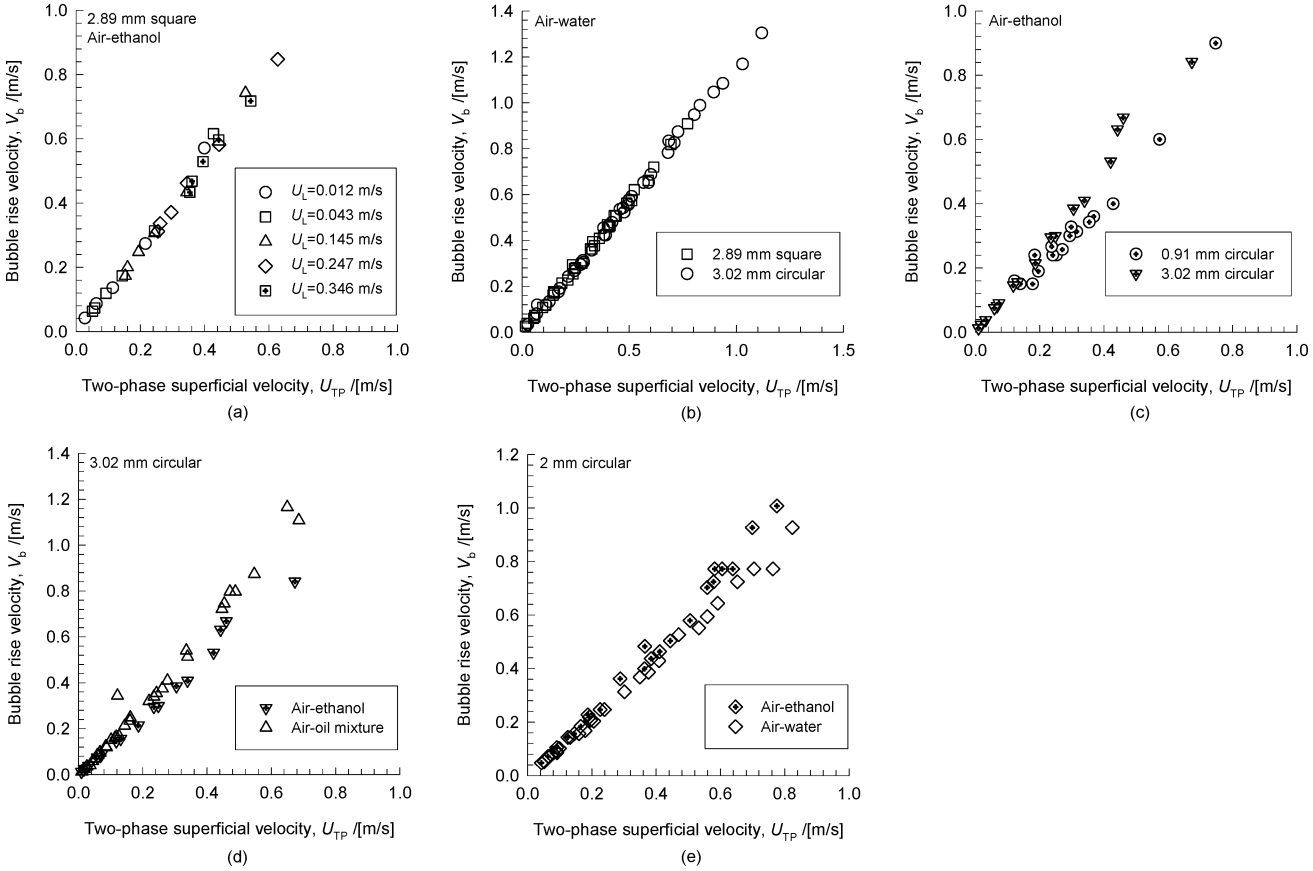

Figure 7. (a) Two-phase superficial velocity (U_{TP}) versus bubble rise velocity (V_b) for the 2.89-mm square capillary air−ethanol system. (b) Influence of capillary geometry on V_b, using air−water data. (c) Influence of capillary scale on V_b, using air−ethanol data. (d) Influence of liquid viscosity on V_b in the 3.02-mm circular capillary. (e) Influence of surface tension on V_b in the 2-mm circular capillary.

the bubble diameter, which is a very difficult hydrodynamic parameter to measure, be estimated. Further discussion on the application of this method for estimating the bubble rise velocity and comparison with the experimental results of this study is available in Appendix II of the Supporting Information accompanying this paper.

To overcome difficulties associated with estimating the bubble diameter, as well as accounting for the effect of liquid properties on bubble rise velocity, the following practical relationship was derived from the correlation of all our experimental data:

$$\frac{V_b}{U_{TP}} = \frac{1}{1 - 0.61Ca^{0.33}} \tag{10}$$

Ca is the capillary number, which is defined as $\mu_L U_{TP}/\sigma$. Figure 8 shows plots of experimental bubble rise velocities, as well as predictions obtained using eq 10 for capillaries of circular and square geometries and different liquids. The fits seem to be very good. The correlation given by eq 10 is valid for predicting V_b in a Ca range of 0.0002−0.39.

3.3. Liquid Slug Length. The liquid slug length is an important hydrodynamic parameter that has been reported to have a very significant effect on gas−liquid mass transfer in capillaries.[21] It has a very complicated relationship to system parameters such as the superficial gas and liquid velocities and fluid properties. To date, only a few experimental correlations for evaluating liquid slug lengths in Taylor flow are available in the literature. One of these, as suggested by Kreutzer[2] and based on the experimental work of Heiszwolf et al.[40] in a 200 cpsi monolith reactor, is

$$\Psi_{slug} = \frac{\epsilon_L}{-0.00141 - 1.556{\epsilon_L}^2 \ln(\epsilon_L)} \tag{11}$$

where Ψ_{slug} is the dimensionless liquid slug length ($\Psi_{slug} = L_{slug}/d_c$) and ϵ_L is the liquid holdup. Laborie et al.[19] studied gas−liquid flow in vertical capillaries and correlated liquid slug length data using the following formula:

$$\Psi_{slug} = 3451\left(\frac{1}{Re'_G E\ddot{o}}\right)^{1.2688} \tag{12}$$

where Re'_G is a gas-phase Reynolds number and $E\ddot{o}$ is the Eötvös number. From observations made during this study, as well as information available in the literature,[2] the liquid slug length would also seem to be influenced by the gas−liquid feed system used. That is to say, for a given superficial gas and liquid velocity, variation in the configuration of the gas−liquid nozzle results in a change in liquid slug length on the same setup. Such complexity makes the development of a generally applicable theoretical model for the prediction of the liquid slug length difficult. However, a correlation would be developed based on the Taylor-flow-regime experimental data obtained in this study and comparisons made with the literature correlations of eqs 11 and 12. As a first step in doing this, reference is made to the vertical capillary mass-transfer study of Bercic et al.,[21] in which the gas−liquid mass-transfer

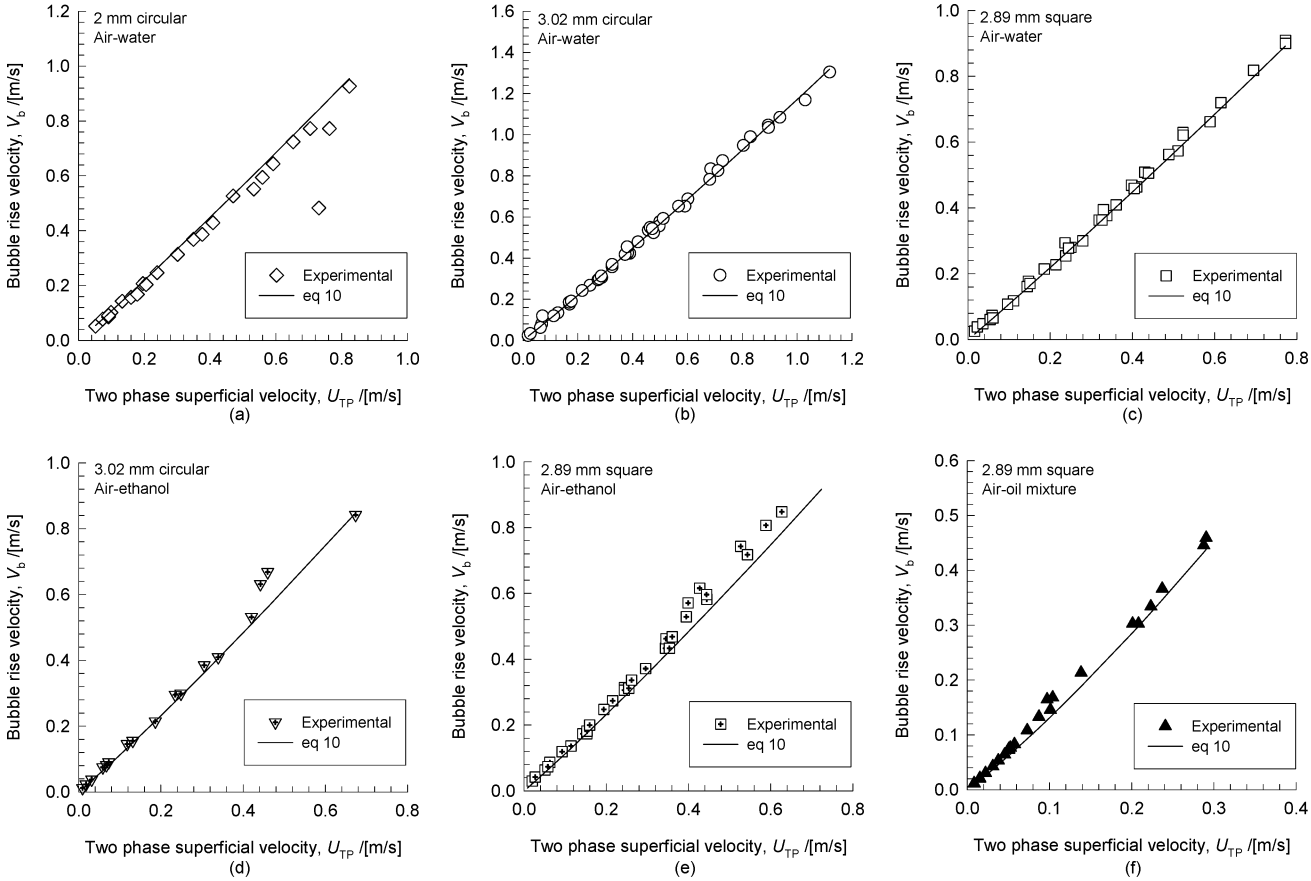

Figure 8. Experimental and predicted bubble rise velocity (V_b) values for different capillary geometries and liquids used: (a) 2-mm circular capillary, air−water; (b) 3.02-mm circular capillary, air−water; (c) 2.89-mm square capillary, air−water; (d) 3.02-mm circular capillary, air−ethanol; (e) 2.89-mm square capillary, air−ethanol; and (f) 2.89-mm square capillary, air−oil mixture.

coefficient (k_La) is expressed as

$$k_La = 0.111\frac{U_{TP}^{1.19}}{L_{slug}^{0.57}} \tag{13}$$

Inspection of eq 13 reveals that the relationship between k_La, U_{TP}, and L_{slug} can approximately be expressed as

$$k_La \sim \frac{U_{TP}}{\sqrt{L_{slug}}} \tag{14}$$

k_La can, in turn, be correlated to the gas-phase and liquid-phase Reynolds numbers. By replacing k_La with the right-hand term in eq 14, and based on the regression of experimental data, the following correlation was obtained:

$$\frac{U_{TP}}{\sqrt{L_{slug}}} = 0.088Re_G^{0.72}Re_L^{0.19} \tag{15}$$

Figure 9 shows plots of experimentally determined liquid slug lengths at varying gas and liquid superficial velocities, as well as predicted slug lengths using eq 15. The predictions seem to be good, although noticeable deviations can be observed in a few cases. Notwithstanding, the predicted slug lengths generally follow the same trends as the experimentally measured values. In Figure 10, experimental dimensionless liquid slug lengths in the Taylor flow regime are compared with predicted values, based on the present study and literature correlations of Laborie et al.[19] (eq 12) and Kreutzer[2] and Heiszwolf et al.[40] (eq 11). Remarkably, an enormous amount of scatter is observed for the literature correlations. The Laborie et al. correlation results in a large scatter distributed above and below the parity line, whereas the Kreutzer−Heiszwolf et al. correlation largely underestimates the experimental data. A possible reason for the latter could be that the gas−liquid flow patterns in the monolith reactor that was used differed greatly from those in the capillary setup used in this study. Besides, the complexity of the liquid slug length and its dependence on such parameters as the configuration of the nozzle likely have a large role in this discrepancy. Further research is thus needed to understand the effect of the gas−liquid feed system on liquid slug length.

3.4. Two-Phase Pressure Drop. Many methods have been proposed for estimating the two-phase frictional pressure drop (ΔP_f) in capillaries. One of these is the Lockhart−Martinelli multiplier method. First proposed by Lockhart and Martinelli,[41] it involves the definition of a two-phase multiplier and a Lockhart−Martinelli parameter. To estimate the frictional pressure drop using this method, a flow-regime-dependent constant that is often called the Chisholm parameter also must be evaluated. From studies in a vertical capillary, Mishima and Hibiki[30] reported that this constant shows a capillary diameter dependence that must be taken into consideration. Furthermore, many investigators have reported on the inability of the Lockhart−Martinelli correlation to predict experimental

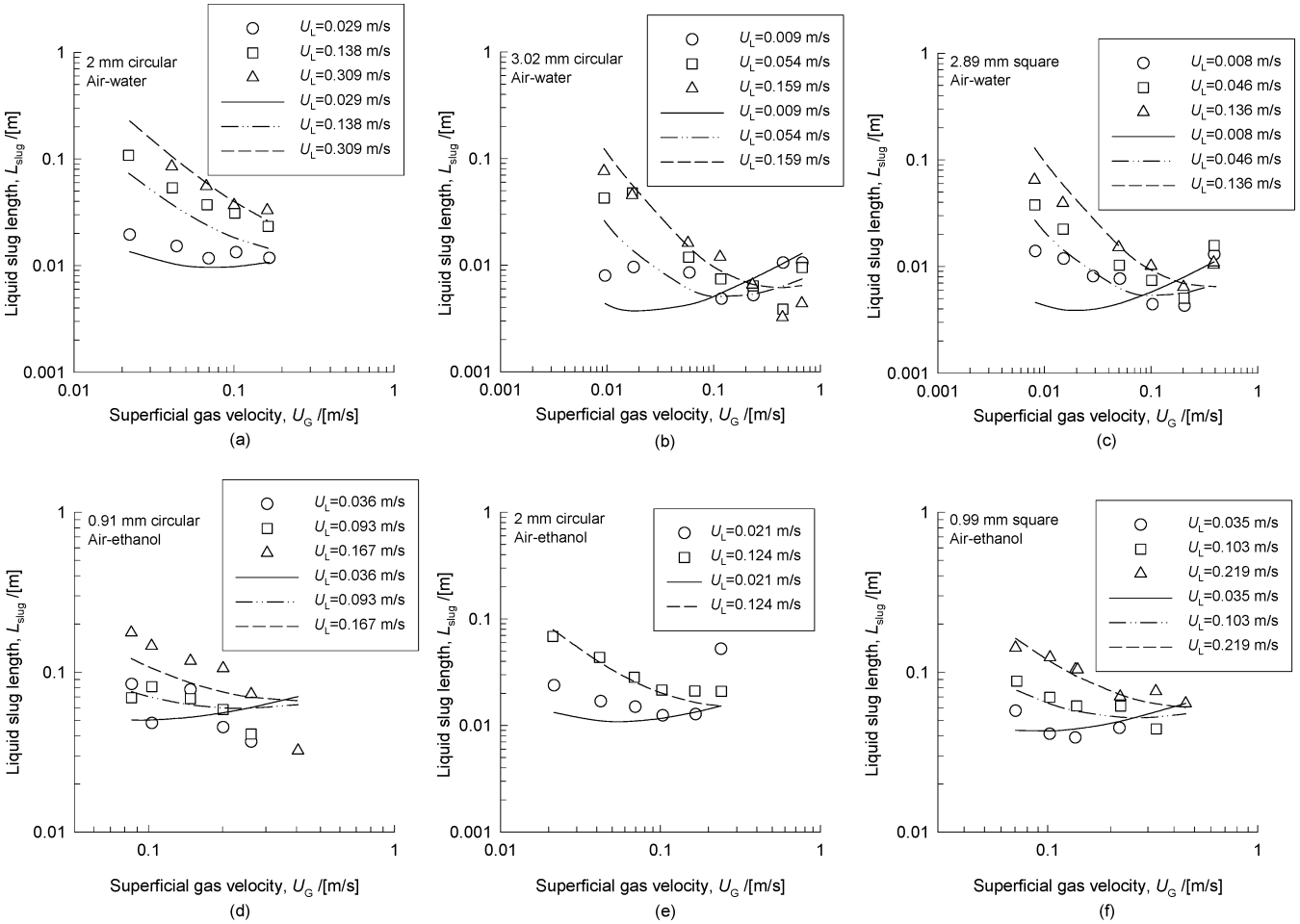

Figure 9. Experimental and predicted liquid slug length (L_{slug}), as a function of superficial gas and liquid velocities: (a) 2-mm circular capillary, air−water; (b) 3.02-mm circular capillary, air−water; (c) 2.89-mm square capillary, air−water; (d) 0.91-mm circular capillary, air−ethanol; (e) 2-mm circular capillary, air−ethanol; and (f) 0.99-mm square capillary, air−ethanol. The closed shapes are experimental data points, whereas the lines represent predicted values using eq 15.

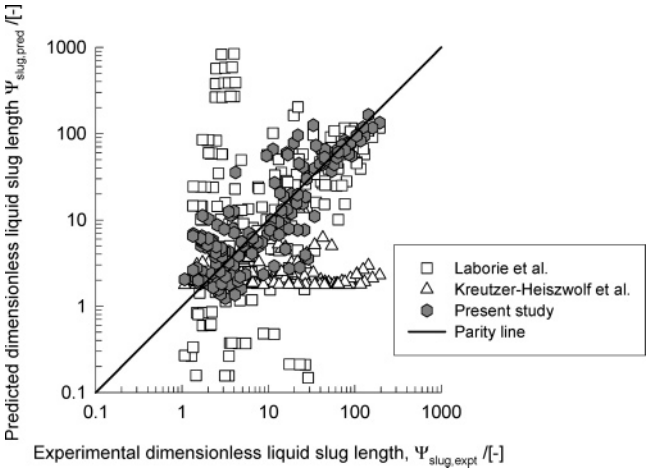

Figure 10. Comparison of experimental dimensionless liquid slug length ($\Psi_{slug,expt}$) with predicted values by various correlations ($\Psi_{slug,pred}$).

pressure drop data, especially at low liquid flow rates.[29,42] Triplett et al.[27] used the homogeneous pressure drop model to calculate ΔP_f, stating that predictions were good in the bubbly and Taylor flow regimes at high Re_L, where, as claimed, the homogeneous flow assumption is applicable. However, significant deviations were reported for slug-annular flow, annular flow, and Taylor flow at relatively low Re_L. One drawback of the Lockhart−Martinelli and homogeneous pressure drop models is the fact that they are flow-regime-independent correlations. This could, to a large extent, account for why they have generally been observed to fail at low liquid flow rates, where, provided an appreciable gas flow ensues (such as in Taylor flow), significant deviation from homogeneous flow occurs. Interestingly, however, it is often at these low liquid flow rates that monolith reactors would typically be operated, i.e., $0.05 < U_G < 0.4$ m/s, depending on the process in question. In view of this, a flow-regime-dependent pressure drop model would be developed based on data obtained from the experimental study undertaken, beginning with a discussion of ΔP_f.

3.4.1. General Observations of Frictional Pressure Drop. For co-current upward two-phase flow in a vertical capillary, the frictional pressure drop can be calculated from the measured total pressure drop, given by

$$\Delta P_T = \Delta P_f + \epsilon_L \rho_L g L_c \tag{16}$$

Figure 11a depicts the frictional pressure drop over the 1.4 m length of the 3.02-mm circular capillary for air−water system at different gas and liquid superficial velocities. Two notable features can be observed from the figure: (1) pressure drop values are negative at lower liquid flow rates, which correspond to the Taylor flow regime; and (2) at higher liquid flow rates, the two-phase frictional pressure drop increases as U_G and U_L

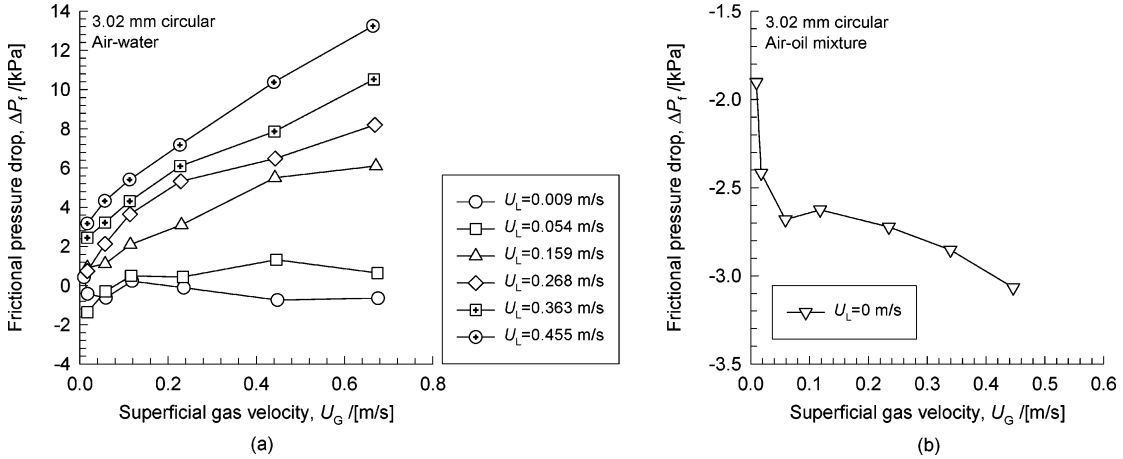

Figure 11. (a) Effect of superficial gas and liquid velocities on frictional pressure drop for the air−water system in the 3.02-mm circular capillary. (b) Frictional pressure drop at zero net liquid flow condition for the air−oil mixture system in the 3.02-mm circular capillary.

increase, but, in the lower-liquid-flow-rate region, changes in the pressure drop do not seem to be regular. Similar trends were observed for other systems that have been investigated. Negative frictional pressure drops in two-phase flows have scarcely been reported in open literature. As can be seen in Appendix I of the Supporting Information accompanying this paper, a negative frictional pressure drop was observed for the bulk of experimental data at very low liquid velocities. In an attempt to understand this phenomenon, experiments were conducted under a zero net liquid flow condition, i.e., liquid was fed batchwise into the capillary while the gas feed was continuous. The result is shown in Figure 11b for an air−oil mixture in the 3.02-mm circular capillary. Observe that, over the range investigated, all frictional pressure drops are negative. As noted by Nicklin,[43] a negative frictional pressure drop means that the total pressure drop is less than the hydrostatic pressure drop, because slip between phases can result in local down flows of liquid, resulting in wall shear stresses that act opposite to the usual sense.

3.4.2. Theoretical Considerations. The apparently complicated behavior of frictional pressure drop, as evidenced previously, requires that, in the development of a correlation for predicting the total pressure drop ΔP_T, negative frictional pressure drop data is taken into account. The extent to which two-phase pressure drops are influenced by flow regimes, fluid properties, and channel geometries also must be considered. With these in mind, the following analysis is provided. Consider, for example, a single-phase vertical tube with liquid flowing in the laminar regime. The total pressure drop is the sum of frictional and static components and can be represented as

$$\Delta P_T = \Delta P_f + \rho_L g L_c \tag{17}$$

In this situation, the frictional pressure drop is given by the Hagen−Poiseuille equation:

$$\Delta P_f = \frac{32\mu_L U_L L_c}{d_c^2} \tag{18}$$

Substitution of eq 18 into eq 17 and rearranging yields

$$\Delta P_T = \frac{32\mu_L L_c}{d_c^2}\left[U_L + \left(\frac{d_c^2}{32\mu_L}\right)\rho_L g\right] \tag{19}$$

By comparing eqs 18 and 19, an equivalent velocity, with respect to the total pressure drop, may be defined as

$$U_e = \left(\frac{d_c^2}{32\mu_L}\right)\rho_L g \tag{20}$$

In subsequent discussions, this velocity will be called the *gravity-equivalent velocity*. It can be considered as the liquid velocity in the capillary that would result in a pressure loss equivalent to the hydrostatic pressure exerted by the liquid phase. Assuming laminar flow for both the gas and liquid phases, the two-phase gravity-equivalent velocity becomes

$$U_e = \left(\frac{d_c^2}{32\mu_L}\right)\epsilon_L\rho_L g \tag{21}$$

and a two-phase mixture velocity U_E, which is defined as the sum of the two-phase superficial velocity (U_{TP}) and the gravity equivalent velocity, is

$$U_E = U_{TP} + U_e \tag{22}$$

A dimensionless two-phase pressure factor F_E can further be defined, analogous to the Fanning friction factor of eq 5:

$$F_E = \frac{\Delta P_T/L_c}{{}^1/_2\rho_L U_E^2(4/d_c)} \tag{23}$$

3.4.3. Correlation of Pressure Drop Data. In a situation where both the gas and liquid-phase flows are laminar, the pressure factor can be expected to take on a form similar to the Fanning friction factor, i.e.,

$$F_E = \frac{C}{Re_E} \tag{24}$$

where Re_E, which is the modified Reynolds number, is defined as

$$Re_E = \frac{\rho_L U_E d_c}{\mu_L} \tag{25}$$

Under this condition, the gas and liquid phases can be viewed as a homogeneous mixture. Based on the discus-

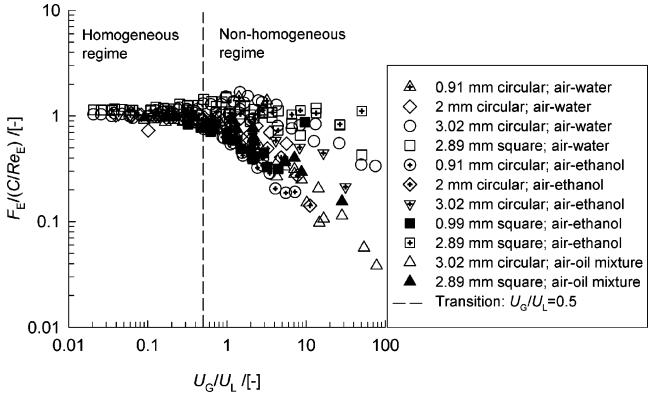

Figure 12. U_G/U_L versus $F_E/(C/Re_E)$, showing that, when $U_G/U_L > 0.5$, the two-phase flow deviates from the homogeneous regime.

sion of the slip ratio S presented previously, it was shown that homogeneous flow generally occurs when $U_G/U_{TP} < 0.5$, which is characterized by a slip ratio S close to unity. A slip ratio of $S > 1$ was shown to indicate deviation from homogeneous flow. Therefore, it can be postulated that a relation between $F_E/(C/Re_E)$ and U_G/U_{TP} (or, equivalently, U_G/U_L) could allow for determination of the transition from homogeneous to nonhomogeneous flow for pressure drop computations. The plot in Figure 12 shows such a relationship, from which the following observations can be made:

(1) For $U_G/U_L < 0.5$, $F_E/(C/Re_E)$ data approach a single line that approximately corresponds to $F_E/(16/Re_E) = 1$ and $F_E/(14.2/Re_E) = 1$ for the circular and square capillaries, respectively, with an uncertainty of approximately ±9%, indicating that the gas and liquid phases can be approximately viewed as a homogeneous mixture. The converse is the case for $U_G/U_L > 0.5$, where significant deviation from homogeneous flow can be observed.

(2) The capillary diameter and liquid viscosity were observed to influence the parameter $F_E/(C/Re_E)$ significantly for $U_G/U_L > 0.5$. This is evidenced by comparing the data of the 0.91-mm, 2-mm, and 3.02-mm circular capillaries for air−ethanol, as well as the data of the 3.02-mm circular and 2.89-mm square capillaries for both the air−oil mixture and air−water system.

Therefore, for homogeneous flow ($U_G/U_L < 0.5$), the total pressure drop can be predicted using eq 24 to first estimate the pressure factor and eq 23 for computing the pressure drop. To predict the total pressure drop when $U_G/U_L > 0.5$, wherein flows deviate from the homogeneous regime, the following analysis was performed. A plot of S versus $F_E/(C/Re_E)$ for $U_G/U_L > 0.5$ is shown in Figure 13a, from which the following dependence was deduced:

$$\frac{F_E}{C/Re_E} \propto S^{-0.5} \tag{26}$$

Through further data analysis, utilizing the parameter $F_E S^{0.5}/(C/Re_E)$ as shown in Figure 13b, the following correlation was obtained:

$$F_E = \frac{C_f}{Re_E} S^{-0.5}[\exp(-0.02Re_E) + 0.07Re_E^{0.34}] \tag{27}$$

Equation 27 provides a convenient way of estimating the nonhomogeneous regime pressure factor, which, when combined with eq 23, allows for the prediction of the total pressure drop. Figure 13c illustrates the comparison of the experimental and correlation-predicted pressure factors, utilizing all experimental data. Note that the predicted pressure factors for $U_G/U_L < 0.5$ were computed with eq 24, whereas eq 27 was used to compute the predicted pressure factors for $U_G/U_L > 0.5$. Figure 14 shows typical experimental and predicted total pressure drop values. The predictions seem to be very good, especially at low and moderate liquid velocities, where Taylor flow occurs. It is also worthy to note that it is at such low liquid velocities that the Lockhart−Martinelli and homogeneous pressure drop models fail to predict the pressure drop, verifying the need for a flow-regime-dependence approach to pressure drop estimation.

4. Conclusions

Two-phase flow hydrodynamics in vertical capillaries with circular and square cross sections that have hydraulic diameters from 0.9 mm to 3 mm were experimentally studied, using air as the gas phase and water, ethanol, or an oil mixture as the liquid phase. Flow regimes, bubble rise velocity, liquid slug length, and pressure drop were investigated, with the gas and liquid superficial velocities being varied in the range of 0.008−1 m/s. Based on the work performed and the discussions presented, the following major conclusions can be drawn:

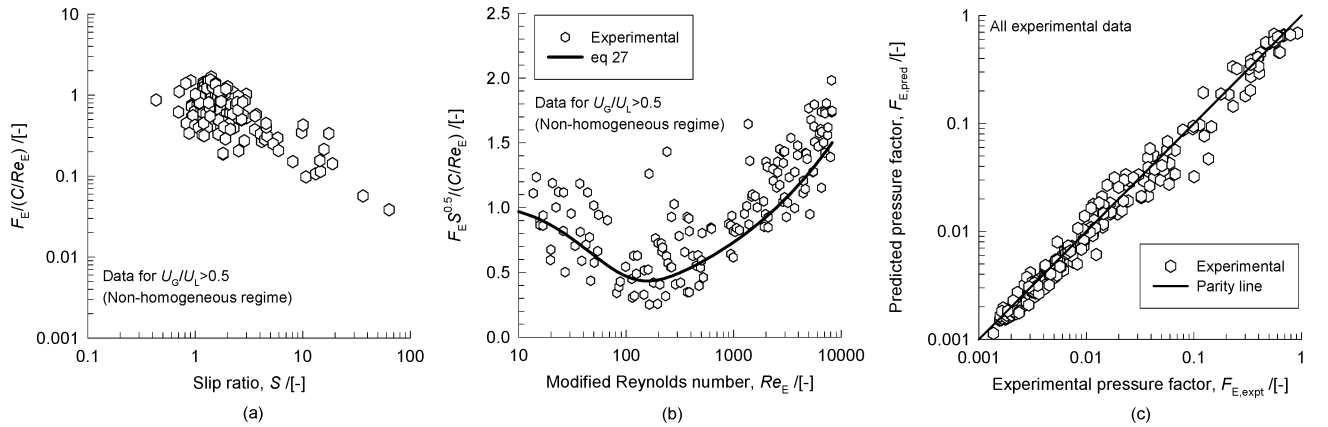

Figure 13. (a) Relationship between the slip ratio S and $F_E/(C/Re_E)$ for $U_G/U_L > 0.5$. (b) Correlation of experimental data for $U_G/U_L > 0.5$ for predicting the pressure factor (F_E). (c) Comparison of pressure factors calculated from experimental pressure drop ($F_{E,expt}$) data with predicted pressure factors ($F_{E,pred}$).

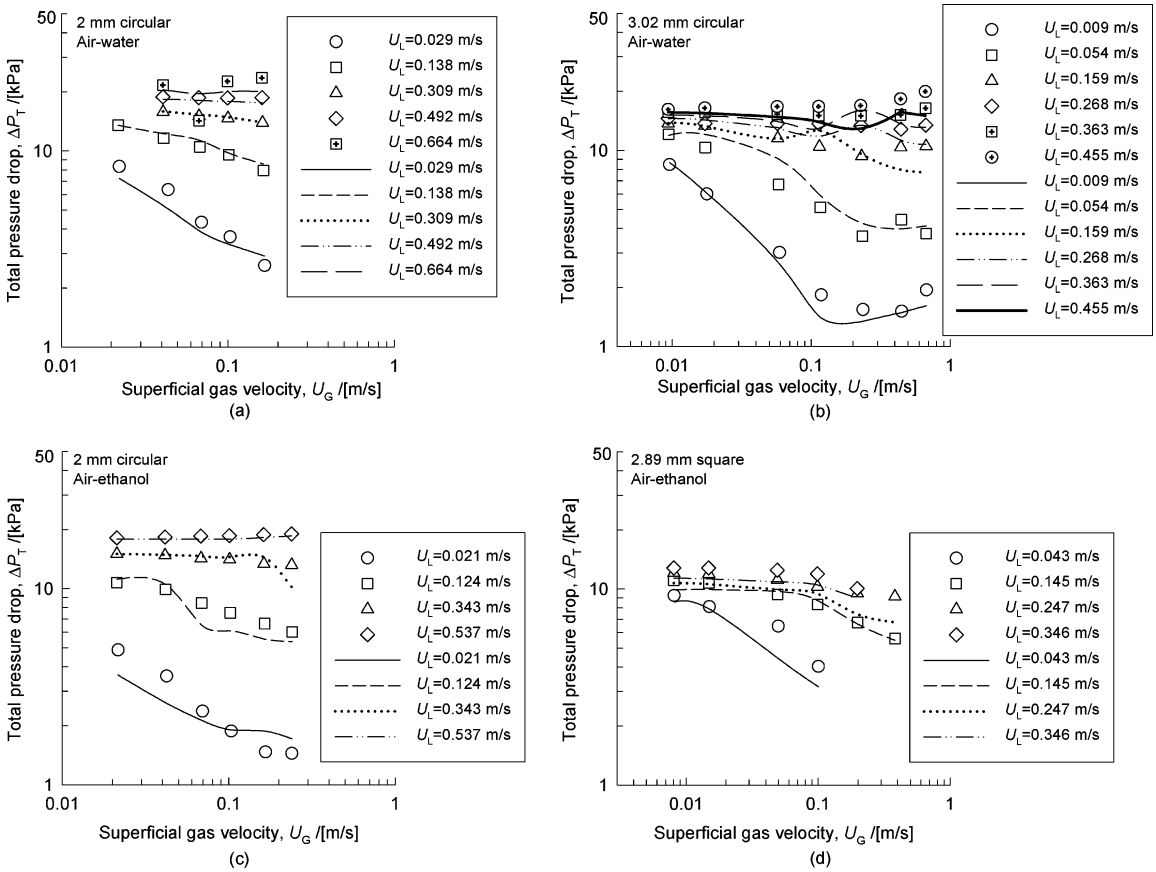

Figure 14. Variation of the experimental and predicted total pressure drop (ΔP_T) with varying superficial gas and liquid velocities: (a) 2-mm circular capillary, air−water; (b) 3.02-mm circular capillary, air−water; (c) 2-mm circular capillary, air−ethanol; and (d) 2.89-mm square capillary, air−ethanol. The closed shapes are experimental data points, whereas the lines represent predicted values.

(1) Within the gas and liquid velocity range under which experiments were conducted, four distinct flow regimes were observed: bubbly, slug-bubbly, Taylor, and churn. A fifth regime, the annular flow regime, occurred at excessively high gas and low liquid velocities.

(2) The slip ratio S was determined to be a useful parameter for gauging the transition from homogeneous to nonhomogeneous flow. It was demonstrated that, when $U_G/U_{TP} < 0.5$, S approaches a value of unity, indicating homogeneous flow. For $U_G/U_{TP} \geq 0.5$, a significant increase in S was observed, indicating significant deviation from homogeneous flow. Moreover, high S values occurred predominantly in the Taylor flow regime.

(3) The influences of capillary geometry, capillary hydraulic diameter, and fluid properties on bubble rise velocity were determined to be of little significance.

(4) A new and simplified correlation for predicting bubble rise velocity and, by implication, the gas holdup in vertical-capillary two-phase flow was proposed.

(5) A correlation for estimating the liquid slug length was developed and was satisfactorily able to predict the experimental liquid slug lengths obtained in this study. However, the fact that existing literature correlations showed an enormous amount of scatter and deviation, when compared to the correlation proposed in this study, leaves open the question as to what extent the configuration of the gas−liquid nozzle (an experimental setup dependent parameter) affects liquid slug lengths in a given setup.

(6) For the prediction of the total pressure drop in a vertical-capillary two-phase flow, a method was proposed based on the definition of the dimensionless pressure factor. Two pressure factor correlations were presented: one for homogeneous flow and the other for nonhomogeneous flow. Based on the analysis of experimental data, a value of $U_G/U_L = 0.5$ was determined to indicate the transition point from homogeneous to nonhomogeneous flow for pressure drop computation. Very good pressure drop predictions were obtained as shown.

Acknowledgment

The Netherlands Foundation for Scientific Research—Chemical Sciences Division (NWO-CW) provides a research program subsidy. One of the authors (H.L.) thanks Beijing University of Chemical Technology, China, for financial support during this work.

Supporting Information Available: Hydrodynamics of Taylor flow in vertical capillaries; flow regimes; bubble rise velocity; liquid slug length; and pressure drop. Appendix I contains the raw experimental data of this study, whereas Appendix II contains further information on correlations for predicting bubble rise velocity (PDF). This material is available free of charge via the Internet at http://pubs.acs.org.

Notation

C = constant relating the Fanning friction factor to laminar flow Reynolds number (also relates the pressure factor to the modified Reynolds number)

d_c = capillary hydraulic diameter (m)

f_b = bubble frequency (s^{-1})
g = gravitational constant (m/s^2)
k_La = gas−liquid mass transfer coefficient (s^{-1})
L_c = length of capillary (m)
L_{slug} = liquid slug length (m)
L_{UC} = unit cell length (m)
P_f = frictional pressure (Pa)
P_T = total pressure (Pa)
S = slip ratio
U_e = gravity-equivalent velocity (m/s)
U_E = two-phase mixture velocity, $U_{TP} + U_e$ (m/s)
U_G = superficial gas velocity (m/s)
U_L = superficial liquid velocity (m/s)
U_{TP} = two-phase superficial velocity, $U_G + U_L$ (m/s)
V_b = bubble rise velocity (m/s)
V_f = liquid film velocity (m/s)
V_L = liquid-phase velocity (m/s)

Greek Symbols

ϵ_L = liquid holdup
ϵ_{Lf} = film liquid holdup
ϵ_G = gas holdup
μ_G = gas viscosity (Pa s)
μ_L = liquid viscosity (Pa s)
ρ_G = gas density (kg/m^3)
ρ_L = liquid density (kg/m^3)
σ = surface tension (N/m)
Ψ_{slug} = dimensionless liquid slug length

Dimensionless Groups

Ca = capillary number, $\mu_L U_{TP}/\sigma$
$Eö$ = Eötvös number, $(\rho_L - \rho_G)d_c^2 g/\sigma$
F_E = pressure factor, $\Delta P_T d_c/(2L_c\rho_L U_E^2)$
f_L = Fanning friction factor, $\Delta P_f d_c/(2L_c\rho_L U_L^2)$
Re_E = modified Reynolds number, $\rho_L U_E d_c/\mu_L$
Re_G = gas-phase Reynolds number, $\rho_G U_G d_c/\mu_G$
Re'_G = gas-phase Reynolds number of Laborie et al.,[19] $\rho_L U_G d_c/\mu_L$
Re_L = liquid-phase Reynolds number, $\rho_L U_L d_c/\mu_L$

Subscripts

expt =experimental
pred = predicted

Literature Cited

(1) Boger, T.; Heibel, A. K.; Sorensen, C. M. Monolithic Catalysts for the Chemical Industry. *Ind. Eng. Chem. Res.* **2004**, *43*, 4602.

(2) Kreutzer, M. T. *Hydrodynamics of Taylor Flow in Capillaries and Monolith Reactors*; Delft University Press: Delft, The Netherlands, 2003.

(3) Roy, S.; Bauer, T.; Al-Dahhan, M. Monoliths as Multiphase Reactors: A Review. *AIChE J.* **2004**, *50* (11), 2918.

(4) Kapteijn, F.; Nijhuis, T. A.; Heiszwolf, J. J.; Moulijn, J. A. New Nontraditional Multiphase Catalytic Reactors Based on Monolithic Structures. *Catal. Today* **2001**, *66*, 133.

(5) Dudukovic, M. P.; Larachi, F.; Mills, P. L. Multiphase Catalytic Reactors: A Perspective on Current Knowledge and Future Trends. *Catal. Rev.—Sci. Eng.* **2002**, *44*, 123.

(6) Nijhuis, T. A.; Kreutzer, M. T.; Romijn, A. C. J.; Kapteijn, F.; Moulijn, J. A., Monolithic Catalysts as Efficient Three-Phase Reactors. *Chem. Eng. Sci.* **2001**, *56*, 823.

(7) Stankiewicz, A. Process Intensification in In-Line Monolithic Reactor. *Chem. Eng. Sci.* **2001**, *56*, 359.

(8) Edvinsson, R. K.; Cybulski, A. A Comparison between the Monolithic Reactor and the Trickle-Bed Reactor for Liquid-Phase Hydrogenations. *Catal. Today* **1995**, *24*, 173.

(9) Smits, H. A.; Stankiewicz, A.; Glasz, W. C.; Fogl, T. H. A.; Moulijn, J. A. Selective Three-Phase Hydrogenation of Unsaturated Hydrocarbons in a Monolithic Reactor. *Chem. Eng. Sci.* **1996**, *51*, 3019.

(10) Boger, T.; Zieverink, M. M. P.; Kreutzer, M. T.; Kapteijn, F.; Moulijn, J.; Addiego, W. P. Monolithic Catalysts as an Alternative to Slurry Systems: Hydrogenation of Edible Oil. *Ind. Eng. Chem. Res.* **2004**, *43*, 2337.

(11) Edvinsson, R.; Irandoust, S. Hydrodesulfurization of Dibenzothiophene in a Monolithic Catalyst Reactor. *Ind. Eng. Chem. Res.* **1993**, *32*, 391.

(12) Klinghoffer, A. A.; Cerro, R. L.; Abraham, M. A. Influence of Flow Properties on the Performance of the Monolith Froth Reactor for Catalytic Wet Oxidation of Acetic Acid. *Ind. Eng. Chem. Res.* **1998**, *37*, 1203.

(13) Kawakami, K.; Kawasaki, K.; Shiraishi, F.; Kusunoki, K. Performance of a Honeycomb Monolith Bioreactor in a Gas−Liquid-Solid Three-Phase System. *Ind. Eng. Chem. Res.* **1989**, *28*, 394.

(14) de Deugd, R. M.; Kapteijn, F.; Moulijn, J. A. Using Monolithic Catalysts for Highly Selective Fischer−Tropsch Synthesis. *Catal. Today* **2003**, *79*, 495.

(15) de Deugd, R. M.; Chougule, R. B.; Kreutzer, M. T.; Meeuse, F. M.; Grievink, J.; Kapteijn, F.; Moulijn, J. A. Is a Monolithic Loop Reactor a Viable Option for Fischer−Tropsch Synthesis? *Chem. Eng. Sci.* **2003**, *58*, 583.

(16) Heibel, A. K.; Scheenen, T. W. J.; Heiszwolf, J. J.; Van As, H.; Kapteijn, F.; Moulijn, J. A. Gas and Liquid-Phase Distribution and Their Effect on Reactor Performance in the Monolith Film Flow Reactor. *Chem. Eng. Sci.* **2001**, *56*, 5935.

(17) Thulasidas, T. C.; Abraham, M. A.; Cerro, R. L. Bubble-Train Flow in Capillaries of Circular and Square Cross-Section. *Chem. Eng. Sci.* **1995**, *50*, 183.

(18) Thulasidas, T. C.; Abraham, M. A.; Cerro, R. L. Dispersion during Bubble-Train Flow in Capillaries. *Chem. Eng. Sci.* **1999**, *54*, 61.

(19) Laborie, S.; Cabassud, C.; Durand-Bourlier, L.; Laine, J. M. Characterisation of Gas−Liquid Two-Phase Flow inside Capillaries. *Chem. Eng. Sci.* **1999**, *54*, 5723.

(20) Irandoust, S.; Andersson, B.; Bengtsson, E.; Siverström, M. Scaling Up of a Monolithic Catalyst Reactor with Two-Phase Flow. *Ind. Eng. Chem. Res.* **1989**, *28*, 1489.

(21) Bercic, G.; Pintar, A. The Role of Gas Bubbles and Liquid Slug Lengths on Mass Transport in the Taylor Flow through Capillaries. *Chem. Eng. Sci.* **1997**, *52*, 3709.

(22) Kreutzer, M. T.; Du, P.; Heiszwolf, J. J.; Kapteijn, F.; Moulijn, J. A. Mass Transfer Characteristics of Three-Phase Monolith Reactors. *Chem. Eng. Sci.* **2001**, *56*, 6015.

(23) Irandoust, S.; Andersson, B. Mass-Transfer and Liquid-Phase Reactions in a Segmented Two-Phase Flow Monolithic Catalyst Reactor. *Chem. Eng. Sci.* **1988**, *43*, 1983.

(24) van Baten, J. M.; Krishna, R. CFD Simulations of Mass Transfer from Taylor Bubbles Rising in Circular Capillaries. *Chem. Eng. Sci.* **2004**, *59*, 2535.

(25) Bercic, G. Influence of Operating Conditions on the Observed Reaction Rate in the Single Channel Monolith Reactor. *Catal. Today* **2001**, *69*, 147.

(26) Triplett, K. A.; Ghiaasiaan, S. M.; Abdel-Khalik, S. I.; Sadowski, D. L. Gas−Liquid Two-Phase Flow in Microchannels—Part I: Two-Phase Flow Patterns. *Int. J. Multiphase Flow* **1999**, *25*, 377.

(27) Triplett, K. A.; Ghiaasiaan, S. M.; Abdel-Khalik, S. I.; LeMouel, A.; McCord, B. N. Gas−Liquid Two-Phase Flow in Microchannels—Part II: Void Fraction and Pressure Drop. *Int. J. Multiphase Flow* **1999**, *25*, 395.

(28) Coleman, J. W.; Garimella, S. Characterization of Two-Phase Flow Patterns in Small Diameter Round and Rectangular Tubes. *Int. J. Heat Mass Transfer* **1999**, *42*, 2869.

(29) Lee, H. J.; Lee, S. Y. Pressure Drop Correlations for Two-Phase Flow within Horizontal Rectangular Channels with Small Heights. *Int. J. Multiphase Flow* **2001**, *27*, 783.

(30) Mishima, K.; Hibiki, T. Some Characteristics of Air−Water Two-Phase Flow in Small Diameter Vertical Tubes. *Int. J. Multiphase Flow* **1996**, *22*, 703.

(31) Wolk, G.; Dreyer, M.; Rath, H. J. Flow Patterns in Small Diameter Vertical Noncircular Channels. *Int. J. Multiphase Flow* **2000**, *26*, 1037.

(32) Zhao, T. S.; Bi, Q. C. Co-current Air−Water Two-Phase Flow Patterns in Vertical Triangular Microchannels. *Int. J. Multiphase Flow* **2001**, *27*, 765.

(33) Chen, I. Y.; Yang, K. S.; Chang, Y. J.; Wang, C. C. Two-Phase Pressure Drop of Air−Water and R-410A in Small Horizontal Tubes. *Int. J. Multiphase Flow* **2001**, *27*, 1293.

(34) Chen, W. L.; Twu, M. C.; Pan, C. Gas−Liquid Two-Phase Flow in Microchannels. *Int. J. Multiphase Flow* **2002**, *28*, 1235.

(35) Vandu, C. O.; Liu, H.; Krishna, R. Taylor Bubble Rise in Circular and Square Capillaries, University of Amsterdam, Amsterdam, The Netherlands, Available at URL http://ct-cr4.chem.uva.nl/SingleCapillary/, accessed June 12, 2004.

(36) Mishima, K.; Ishii, M. Flow Regime Transition Criteria for Upward Two-Phase Flow in Vertical Tubes. *Int. J. Heat Mass Transfer* **1984**, *27*, 723.

(37) Suo, M. Two Phase Flow in Capillary Tubes, D.Sc. Thesis, Massachusetts Institute of Technology, Cambridge, MA, 1963.

(38) Fukano, T.; Kariyasaki, A. Characteristics of Gas−Liquid 2-Phase Flow in a Capillary-Tube. *Nucl. Eng. Des.* **1993**, *141*, 59.

(39) Barnea, D. Effect of Bubble Shape on Pressure Drop Calculations in Vertical Slug Flow. *Int. J. Multiphase Flow* **1990**, *16*, 79.

(40) Heiszwolf, J. J.; Kreutzer, M. T.; van den Eijnden, M. G.; Kapteijn, F.; Moulijn, J. A. Gas−Liquid Mass Transfer of Aqueous Taylor Flow in Monoliths. *Catal. Today* **2001**, *69*, 51.

(41) Lockhart, R. W.; Martinelli, R. C. Proposed Correlation of Data for Isothermal Two-Phase, Two-Component Flow in Pipes. *Chem. Eng. Prog.* **1949**, *45*, 39.

(42) Zhao, T. S.; Bi, Q. C. Pressure Drop Characteristics of Gas−Liquid Two-Phase Flow in Vertical Miniature Triangular Channels. *Int. J. Heat Mass Transfer* **2001**, *44*, 2523.

(43) Nicklin, D. J. Two-Phase Bubble Flow. *Chem. Eng. Sci.* **1962**, *17*, 693.

Received for review August 3, 2004
Revised manuscript received September 20, 2004
Accepted September 30, 2004

IE049307N

Hydrodynamics of Taylor Flow in Vertical Capillaries: Flow Regimes, Bubble Rise Velocity, Liquid Slug Length and Pressure Drop

(Supplementary Information)[†]

Hui Liu, Chippla O. Vandu and Rajamani Krishna*

Van 't Hoff Institute for Molecular Sciences, University of Amsterdam, Nieuwe Achtergracht 166,

1018 WV Amsterdam, The Netherlands.

*Corresponding author: Tel.: +31-20-525-7007; fax: +31-20-525-5604; Email: R.Krishna@uva.nl

[†]This is a web-published supplement to the paper entitled "Hydrodynamics of Taylor Flow in Vertical Capillaries: Flow Regimes, Bubble Rise Velocity, Liquid Slug Length and Pressure Drop" by Liu, Vandu and Krishna.

APPENDIX I: Raw Experimental Data

Campaign 1 (0.91 mm circular capillary; air-water system)

U_G /[m/s]	U_L /[m/s]	V_b /[m/s]	f_b /[s^{-1}]	ΔP_T /[Pa]	ε_G /[-]	L_{UC} /[m]	L_{slug} /[m]	ΔP_f /[Pa]	Flow regime
0.089	0.028	0.112	32.6	12236	0.796	0.0034	0.0007	9446	Taylor
0.086	0.061	0.141	44.9	19378	0.609	0.0031	0.0012	14022	Taylor
0.157	0.061	0.218	50.5	15411	0.720	0.0043	0.0012	11578	Taylor
0.157	0.061	0.200	53.9	15600	0.785	0.0037	0.0008	12655	Taylor
0.103	0.127	0.248	8.1	17182	0.415	0.0306	0.0179	9169	Taylor
0.150	0.127	0.288	13.4	16308	0.522	0.0215	0.0103	9750	Taylor
0.087	0.143	0.240	7.7	18210	0.361	0.0312	0.0199	9451	Taylor
0.086	0.308	0.411	7.8	27390	0.209	0.0529	0.0419	16542	Taylor
0.086	0.308	0.356	8.9	27394	0.241	0.0402	0.0305	16989	Taylor
0.106	0.308	0.436	8.3	27389	0.243	0.0528	0.0400	17020	Taylor
0.156	0.308	0.480	10.8	27275	0.325	0.0446	0.0301	18019	Taylor

Campaign 2 (2 mm circular capillary; air-water system)

U_G /[m/s]	U_L /[m/s]	V_b /[m/s]	f_b /[s^{-1}]	ΔP_T /[Pa]	ε_G /[-]	L_{UC} /[m]	L_{slug} /[m]	ΔP_f /[Pa]	Flow regime
0.022	0.029	0.052	1.5	8337	0.428	0.0341	0.0195	494	Taylor
0.044	0.029	0.077	2.2	6358	0.568	0.0352	0.0152	441	Taylor
0.069	0.029	0.102	2.8	4336	0.684	0.0369	0.0117	0	Taylor
0.103	0.029	0.143	3.0	3648	0.721	0.0478	0.0133	-171	Taylor
0.167	0.029	0.207	3.4	2606	0.805	0.0604	0.0118	-66	Taylor
0.022	0.069	0.086	1.4	11295	0.258	0.0611	0.0454	1120	Taylor
0.022	0.069	0.091	1.4	11279	0.244	0.0664	0.0502	918	Taylor
0.022	0.138	0.157	1.2	13548	0.140	0.1259	0.1082	1763	Taylor
0.041	0.138	0.168	2.4	11624	0.245	0.0711	0.0536	1282	Taylor
0.068	0.138	0.203	3.6	10504	0.334	0.0558	0.0371	1381	Taylor
0.101	0.138	0.247	4.7	9556	0.411	0.0526	0.0310	1481	Taylor
0.164	0.138	0.313	6.4	7964	0.523	0.0489	0.0233	1422	Taylor
0.041	0.309	0.368	3.8	15796	0.111	0.0956	0.0850	3614	Taylor
0.067	0.309	0.386	5.8	15072	0.174	0.0672	0.0555	3753	Taylor
0.100	0.309	0.429	8.9	14701	0.234	0.0481	0.0369	4196	Taylor
0.162	0.309	0.527	11.1	13944	0.307	0.0476	0.0330	4442	Taylor
0.041	0.492	0.552	6.5	18866	0.074	0.0846	0.0783	6174	Taylor
0.067	0.492	0.594	8.7	18678	0.113	0.0680	0.0603	6518	Taylor
0.100	0.492	0.644	14.2	18622	0.155	0.0455	0.0384	7039	Slug-bubbly
0.161	0.492	0.724	18.1	18705	0.222	0.0400	0.0311	8041	Taylor
0.041	0.664	0.773	11.3	21698	0.053	0.0683	0.0647	8715	Slug-bubbly
0.067	0.664	0.483	11.0	14264	0.139	0.0438	0.0377	2464	Taylor
0.100	0.664	0.773	21.9	22623	0.129	0.0353	0.0308	10683	Slug-bubbly
0.160	0.664	0.927	n/a	23596	0.173	n/a	n/a	12259	Slug-bubbly

Campaign 3 (3.02 mm circular capillary; air-water system)

U_G /[m/s]	U_L /[m/s]	V_b /[m/s]	f_b /[s^{-1}]	ΔP_T /[Pa]	ε_G /[-]	L_{UC} /[m]	L_{slug} /[m]	ΔP_f /[Pa]	Flow regime
0.010	0.009	0.023	1.7	8458	0.414	0.0136	0.0080	427	Taylor
0.018	0.009	0.033	1.6	6000	0.532	0.0204	0.0096	-418	Taylor
0.059	0.009	0.081	2.5	3014	0.735	0.0321	0.0085	-624	Taylor
0.118	0.009	0.134	3.2	1834	0.883	0.0415	0.0048	234	Taylor
0.236	0.009	0.268	6.2	1546	0.879	0.0433	0.0052	-111	Taylor
0.448	0.009	0.536	8.3	1513	0.836	0.0643	0.0105	-735	Taylor
0.676	0.009	0.833	14.9	1943	0.811	0.0558	0.0105	-645	Churn
0.009	0.054	0.062	1.2	12102	0.151	0.0502	0.0426	467	Taylor
0.017	0.054	0.119	2.1	10359	0.145	0.0556	0.0475	-1359	Taylor
0.058	0.054	0.119	5.1	6703	0.490	0.0233	0.0119	-292	Taylor
0.116	0.054	0.176	8.0	5134	0.662	0.0219	0.0074	500	Taylor
0.234	0.054	0.305	11.2	3655	0.766	0.0273	0.0064	450	Taylor
0.446	0.054	0.577	33.9	4438	0.772	0.0170	0.0039	1319	Taylor
0.675	0.054	0.874	21.0	3764	0.772	0.0416	0.0095	643	Churn
0.009	0.159	0.185	2.3	13750	0.051	0.0803	0.0763	736	Taylor
0.017	0.159	0.191	3.8	13391	0.090	0.0499	0.0454	920	Slug-bubbly
0.057	0.159	0.242	11.4	11563	0.237	0.0212	0.0162	1106	Slug-bubbly
0.115	0.159	0.294	15.0	10465	0.389	0.0196	0.0120	2096	Taylor
0.231	0.159	0.423	29.3	9325	0.546	0.0144	0.0066	3096	Taylor
0.442	0.159	0.687	75.5	10392	0.644	0.0091	0.0032	5507	Taylor
0.671	0.159	0.989	72.5	10508	0.679	0.0136	0.0044	6103	Churn
0.009	0.268	0.300	3.0	14568	0.031	0.1004	0.0972	1288	Slug-bubbly
0.017	0.268	0.313	5.1	13696	0.055	0.0617	0.0583	743	Bubbly
0.057	0.268	0.357	15.1	13774	0.160	0.0236	0.0199	2258	Slug-bubbly
0.057	0.268	0.369	16.3	13712	0.155	0.0226	0.0191	2128	Slug-bubbly
0.114	0.268	0.425	25.4	13676	0.268	0.0167	0.0123	3641	Slug-bubbly
0.229	0.268	0.556	49.5	13391	0.412	0.0112	0.0066	5325	Slug-bubbly
0.443	0.268	0.826	85.4	12834	0.537	0.0097	0.0045	6481	Slug-bubbly
0.669	0.268	1.084	98.1	13450	0.617	0.0111	0.0042	8198	Churn
0.009	0.363	0.417	5.1	15669	0.022	0.0810	0.0792	2270	Slug-bubbly
0.017	0.363	0.455	6.8	15635	0.038	0.0667	0.0642	2446	Bubbly
0.057	0.363	0.479	20.2	15287	0.119	0.0237	0.0209	3211	Bubbly
0.113	0.363	0.523	35.3	15050	0.217	0.0148	0.0116	4311	Slug-bubbly
0.228	0.363	0.652	75.4	15013	0.349	0.0087	0.0056	6093	Bubbly
0.441	0.363	0.947	69.3	15187	0.466	0.0137	0.0073	7862	Slug-bubbly
0.666	0.363	1.169	121.4	16413	0.570	0.0096	0.0041	10519	Churn
0.009	0.455	0.549	11.2	16175	0.017	0.0490	0.0481	2701	Bubbly
0.017	0.455	0.542	14.1	16440	0.032	0.0384	0.0372	3167	Bubbly
0.057	0.455	0.592	30.6	16706	0.096	0.0193	0.0175	4315	Bubbly
0.113	0.455	0.652	52.9	16737	0.173	0.0123	0.0102	5406	Bubbly
0.227	0.455	0.783	86.9	16909	0.290	0.0090	0.0064	7176	Bubbly
0.440	0.455	1.047	96.0	18319	0.420	0.0109	0.0063	10373	Slug-bubbly
0.441	0.455	1.034	123.9	18286	0.426	0.0083	0.0048	10417	Slug-bubbly
0.664	0.455	1.304	171.2	19968	0.509	0.0076	0.0037	13241	Churn

Campaign 4 (2.89 mm square capillary; air-water system)

U_G /[m/s]	U_L /[m/s]	V_b /[m/s]	f_b /[s^{-1}]	ΔP_T /[Pa]	ε_G /[-]	L_{UC} /[m]	L_{slug} /[m]	ΔP_f /[Pa]	Flow regime
0.008	0.008	0.026	1.2	9037	0.322	0.0206	0.0140	-260	Taylor
0.015	0.008	0.038	1.9	7604	0.397	0.0197	0.0119	-658	Taylor
0.029	0.008	0.048	2.4	4918	0.597	0.0201	0.0081	-605	Taylor
0.051	0.008	0.074	2.9	3389	0.694	0.0251	0.0077	-801	Taylor
0.103	0.008	0.118	3.4	2409	0.874	0.0352	0.0044	685	Taylor
0.206	0.008	0.227	5.0	1725	0.906	0.0458	0.0043	442	Taylor
0.391	0.008	0.469	6.0	1630	0.834	0.0787	0.0130	-639	Taylor
0.008	0.046	0.061	1.4	12045	0.134	0.0437	0.0379	172	Taylor
0.015	0.046	0.066	2.3	11059	0.228	0.0291	0.0224	481	Taylor
0.050	0.046	0.108	5.6	7073	0.469	0.0193	0.0103	-206	Taylor
0.101	0.046	0.177	10.2	6755	0.572	0.0173	0.0074	887	Taylor
0.204	0.046	0.280	15.1	4937	0.729	0.0186	0.0050	1220	Taylor
0.391	0.046	0.506	7.3	3107	0.773	0.0693	0.0157	-10	Taylor
0.008	0.136	0.161	2.4	13730	0.050	0.0685	0.0651	711	Slug-bubbly
0.015	0.136	0.170	3.9	13388	0.087	0.0432	0.0394	879	Taylor
0.050	0.136	0.214	10.9	11459	0.232	0.0197	0.0151	932	Taylor
0.100	0.136	0.294	19.2	11213	0.340	0.0153	0.0101	2163	Taylor
0.202	0.136	0.377	27.3	8710	0.536	0.0138	0.0064	2350	Taylor
0.387	0.136	0.629	23.4	7495	0.615	0.0269	0.0104	2219	Slug-bubbly
0.387	0.136	0.621	21.4	7532	0.624	0.0290	0.0109	2378	Slug-bubbly
0.008	0.230	0.254	3.1	14468	0.032	0.0817	0.0791	1197	Bubbly
0.015	0.230	0.278	5.9	14259	0.054	0.0473	0.0448	1286	Bubbly
0.050	0.230	0.300	13.6	13292	0.165	0.0220	0.0184	1847	Slug-bubbly
0.099	0.230	0.395	21.5	13321	0.252	0.0183	0.0137	3067	Slug-bubbly
0.200	0.230	0.508	40.0	12661	0.394	0.0127	0.0077	4354	Slug-bubbly
0.385	0.230	0.720	34.6	10534	0.535	0.0208	0.0097	4162	Slug-bubbly
0.008	0.311	0.363	6.3	15140	0.022	0.0573	0.0560	1739	Bubbly
0.015	0.311	0.363	5.5	15119	0.041	0.0658	0.0631	1974	Bubbly
0.049	0.311	0.409	15.0	14495	0.121	0.0273	0.0240	2443	Slug-bubbly
0.099	0.311	0.464	23.5	14317	0.214	0.0198	0.0155	3538	Slug-bubbly
0.200	0.311	0.573	47.1	14039	0.349	0.0122	0.0079	5109	Slug-bubbly
0.384	0.311	0.818	39.4	13053	0.469	0.0208	0.0110	5774	Slug-bubbly
0.008	0.390	0.469	9.5	15738	0.017	0.0496	0.0487	2268	Bubbly
0.015	0.390	0.459	13.0	15808	0.032	0.0352	0.0341	2545	Bubbly
0.049	0.390	0.506	21.7	15669	0.098	0.0233	0.0210	3299	Bubbly
0.099	0.390	0.563	28.6	15758	0.176	0.0197	0.0162	4461	Slug-bubbly
0.199	0.390	0.662	56.6	15987	0.301	0.0117	0.0082	6403	Bubbly
0.383	0.390	0.909	60.8	15662	0.421	0.0149	0.0087	7724	Slug-bubbly
0.383	0.390	0.900	63.3	15863	0.425	0.0142	0.0082	7986	Slug-bubbly

Campaign 5 (0.91 mm circular capillary; air-ethanol system)

U_G /[m/s]	U_L /[m/s]	V_b /[m/s]	f_b /[s^{-1}]	ΔP_T /[Pa]	ε_G /[-]	L_{UC} /[m]	L_{slug} /[m]	ΔP_f /[Pa]	Flow regime
0.085	0.036	0.160	0.9	5641	0.534	0.1808	0.0843	647	Taylor
0.103	0.036	0.150	1.0	4899	0.688	0.1540	0.0481	1555	Taylor
0.148	0.036	0.240	1.2	3302	0.617	0.2032	0.0778	-798	Taylor
0.201	0.036	0.267	1.4	3372	0.754	0.1840	0.0453	736	Taylor
0.262	0.036	0.327	1.8	4104	0.800	0.1833	0.0367	1957	Taylor
0.085	0.093	0.150	0.9	9995	0.569	0.1605	0.0693	5373	Taylor
0.103	0.093	0.189	1.1	9503	0.544	0.1785	0.0813	4623	Taylor
0.148	0.093	0.240	1.3	8334	0.617	0.1784	0.0683	4231	Taylor
0.201	0.093	0.300	1.7	8882	0.670	0.1768	0.0584	5344	Taylor
0.262	0.093	0.343	2.0	8648	0.763	0.1730	0.0410	6107	Taylor
0.085	0.167	0.240	0.9	17530	0.355	0.2739	0.1768	10616	Taylor
0.103	0.167	0.257	1.1	17244	0.400	0.2434	0.1460	10819	Taylor
0.148	0.167	0.313	1.4	16437	0.473	0.2233	0.1177	10792	Taylor
0.201	0.167	0.360	1.5	15866	0.558	0.2400	0.1060	11136	Taylor
0.262	0.167	0.400	1.9	14155	0.654	0.2107	0.0729	10449	Taylor
0.406	0.167	0.600	6.0	13140	0.676	0.1000	0.0324	9674	Taylor
0.580	0.167	0.900	n/a	15017	0.645	n/a	n/a	11214	Slug-bubbly

Campaign 6 (2 mm circular capillary; air-ethanol system)

U_G /[m/s]	U_L /[m/s]	V_b /[m/s]	f_b /[s^{-1}]	ΔP_T /[Pa]	ε_G /[-]	L_{UC} /[m]	L_{slug} /[m]	ΔP_f /[Pa]	Flow regime
0.022	0.021	0.048	1.1	4878	0.453	0.0435	0.0238	-980	Taylor
0.042	0.021	0.072	1.8	3592	0.589	0.0411	0.0169	-815	Taylor
0.070	0.021	0.105	2.4	2375	0.664	0.0445	0.0150	-1223	Taylor
0.104	0.021	0.143	3.2	1881	0.724	0.0450	0.0124	-1079	Taylor
0.166	0.021	0.227	4.8	1471	0.731	0.0475	0.0128	-1406	Taylor
0.239	0.021	0.644	7.7	1449	0.372	0.0833	0.0524	-5284	Taylor
0.021	0.058	0.084	1.5	8231	0.255	0.0569	0.0424	251	Taylor
0.021	0.124	0.157	2.0	10749	0.136	0.0793	0.0685	1494	Taylor
0.042	0.124	0.184	3.3	9907	0.227	0.0563	0.0435	1622	Taylor
0.069	0.124	0.219	5.3	8448	0.314	0.0413	0.0284	1099	Taylor
0.102	0.124	0.247	6.7	7537	0.414	0.0366	0.0214	1261	Taylor
0.164	0.124	0.362	9.4	6629	0.454	0.0386	0.0211	780	Taylor
0.241	0.124	0.483	11.6	6023	0.499	0.0417	0.0209	656	Taylor
0.021	0.343	0.400	n/a	15050	0.053	n/a	n/a	4908	Bubbly
0.041	0.343	0.437	n/a	14803	0.095	n/a	n/a	5107	Slug-bubbly
0.068	0.343	0.464	n/a	14285	0.147	n/a	n/a	5147	Slug-bubbly
0.101	0.343	0.504	n/a	14105	0.201	n/a	n/a	5544	Slug-bubbly
0.163	0.343	0.579	n/a	13419	0.281	n/a	n/a	5717	Slug-bubbly
0.239	0.343	0.773	n/a	13241	0.309	n/a	n/a	5843	Slug-bubbly
0.021	0.537	0.702	n/a	18173	0.030	n/a	n/a	7785	Bubbly
0.041	0.537	0.724	n/a	18353	0.057	n/a	n/a	8253	Bubbly
0.068	0.537	0.773	n/a	18541	0.088	n/a	n/a	8771	Bubbly
0.101	0.537	0.773	n/a	18661	0.131	n/a	n/a	9348	Bubbly
0.162	0.537	0.927	n/a	18856	0.175	n/a	n/a	10018	Slug-bubbly
0.238	0.537	1.008	n/a	19027	0.236	n/a	n/a	10848	Slug-bubbly

Campaign 7 (3.02 mm circular capillary; air-ethanol system)

U_G /[m/s]	U_L /[m/s]	V_b /[m/s]	f_b /[s^{-1}]	ΔP_T /[Pa]	ε_G /[-]	L_{UC} /[m]	L_{slug} /[m]	ΔP_f /[Pa]	Flow regime
0.010	0.000	0.012	0.1	209	0.800	0.0853	0.0170	-1929	Taylor
0.018	0.000	0.023	0.3	261	0.769	0.0683	0.0158	-2215	Taylor
0.059	0.000	0.075	1.1	336	0.785	0.0678	0.0146	-1966	Taylor
0.118	0.000	0.146	1.9	373	0.811	0.0777	0.0147	-1654	Taylor
0.235	0.000	0.295	3.0	536	0.796	0.0993	0.0202	-1649	Churn
0.339	0.000	0.409	n/a	783	0.829	n/a	n/a	-1050	Churn
0.442	0.000	0.631	n/a	831	0.700	n/a	n/a	-2378	Churn
0.673	0.000	0.842	n/a	781	0.800	n/a	n/a	-1359	Churn
0.018	0.014	0.038	1.9	4701	0.464	0.0198	0.0106	-1040	Taylor
0.059	0.014	0.090	4.5	2437	0.651	0.0198	0.0069	-1303	Taylor
0.117	0.014	0.156	8.2	1713	0.755	0.0190	0.0046	-914	Taylor
0.234	0.014	0.299	15.9	1687	0.784	0.0188	0.0041	-626	Taylor
0.446	0.014	0.668	2.6	1342	0.667	0.2614	0.0871	-2228	Churn
0.017	0.050	0.081	4.1	8420	0.214	0.0198	0.0155	3	Taylor
0.017	0.169	0.214	6.1	10783	0.081	0.0349	0.0321	937	Slug-bubbly
0.017	0.288	0.385	n/a	12279	0.045	n/a	n/a	2049	Bubbly
0.017	0.403	0.532	n/a	13263	0.033	n/a	n/a	2899	Bubbly

Campaign 8 (0.99 mm square capillary; air-ethanol system)

U_G /[m/s]	U_L /[m/s]	V_b /[m/s]	f_b /[s^{-1}]	ΔP_T /[Pa]	ε_G /[-]	L_{UC} /[m]	L_{slug} /[m]	ΔP_f /[Pa]	Flow regime
0.070	0.035	0.133	1.1	4508	0.528	0.1213	0.0573	-551	Taylor
0.102	0.035	0.144	1.0	4221	0.710	0.1421	0.0411	1119	Taylor
0.136	0.035	0.200	1.7	n/a	0.678	0.1211	0.0391	n/a	Taylor
0.220	0.035	0.327	2.4	n/a	0.671	0.1365	0.0449	n/a	Taylor
0.326	0.035	n/a	14.7	n/a	n/a	n/a	n/a	n/a	Taylor
0.337	0.035	0.352	12.0	16115	0.957	0.0292	0.0013	15656	Taylor
0.451	0.035	0.320	n/a	n/a	1.410	n/a	n/a	n/a	Taylor-churn
0.458	0.035	n/a	n/a	5344	n/a	n/a	n/a	n/a	Taylor-churn
0.938	0.035	n/a	n/a	7121	n/a	n/a	n/a	n/a	Churn
1.792	0.035	n/a	n/a	9431	n/a	n/a	n/a	n/a	Churn
2.808	0.035	n/a	n/a	10469	n/a	n/a	n/a	n/a	Churn
3.572	0.035	n/a	n/a	11014	n/a	n/a	n/a	n/a	Churn
0.071	0.102	0.178	1.2	10587	0.401	0.1470	0.0880	4173	Taylor
0.103	0.102	0.218	1.7	10267	0.470	0.1315	0.0697	4589	Taylor
0.137	0.102	0.267	2.1	9593	0.516	0.1270	0.0615	4404	Taylor
0.223	0.102	0.400	2.9	8245	0.557	0.1387	0.0614	3503	Taylor
0.329	0.102	0.497	3.8	7969	0.663	0.1313	0.0442	4361	Taylor
0.455	0.102	0.579	13.2	9187	0.786	0.0440	0.0094	6893	Taylor-churn
0.070	0.219	0.277	1.5	17577	0.254	0.1908	0.1423	9589	Taylor
0.103	0.219	0.351	2.0	17375	0.292	0.1748	0.1238	9792	Taylor
0.136	0.219	0.400	2.5	16736	0.339	0.1580	0.1044	9659	Taylor
0.139	0.219	0.400	2.5	n/a	0.347	0.1592	0.1039	n/a	Taylor
0.222	0.219	0.480	3.7	16058	0.462	0.1306	0.0703	10291	Taylor
0.328	0.219	0.686	4.7	15472	0.478	0.1456	0.0760	9881	Taylor
0.454	0.219	0.835	6.0	15092	0.544	0.1398	0.0638	10207	Taylor
0.460	0.219	0.960	5.7	14891	0.479	0.1688	0.0879	9313	Slug-bubbly
0.958	0.219	n/a	n/a	18870	n/a	n/a	n/a	n/a	Slug-bubbly

Campaign 9 (2.89 mm square capillary; air-ethanol system)

U_G /[m/s]	U_L /[m/s]	V_b /[m/s]	f_b /[s^{-1}]	ΔP_T /[Pa]	ε_G /[-]	L_{UC} /[m]	L_{slug} /[m]	ΔP_f /[Pa]	Flow regime
0.008	0.000	n/a	0.8	4458	n/a	n/a	n/a	n/a	Taylor
0.015	0.000	n/a	1.3	n/a	n/a	n/a	n/a	n/a	Taylor
0.050	0.000	n/a	1.6	n/a	n/a	n/a	n/a	n/a	Taylor
0.100	0.000	n/a	1.4	n/a	n/a	n/a	n/a	n/a	Taylor
0.199	0.000	n/a	1.6	n/a	n/a	n/a	n/a	n/a	Taylor
0.288	0.000	n/a	1.2	n/a	n/a	n/a	n/a	n/a	Taylor
0.378	0.000	n/a	1.9	n/a	n/a	n/a	n/a	n/a	Taylor
0.572	0.000	n/a	1.3	n/a	n/a	n/a	n/a	n/a	Taylor
0.579	0.000	n/a	1.3	n/a	n/a	n/a	n/a	n/a	Taylor
0.008	0.012	0.030	1.3	6810	0.272	0.0237	0.0172	-990	Taylor
0.015	0.012	0.042	2.1	5525	0.360	0.0201	0.0129	-1333	Taylor
0.051	0.012	0.087	4.3	n/a	0.584	0.0200	0.0083	n/a	Taylor
0.102	0.012	0.136	3.7	n/a	0.750	0.0369	0.0092	n/a	Taylor
0.204	0.012	0.274	2.1	n/a	0.744	0.1314	0.0336	n/a	Taylor
0.387	0.012	0.571	2.4	n/a	0.678	0.2397	0.0772	n/a	Taylor
0.576	0.012	0.807	1.9	n/a	0.714	0.4339	0.1241	n/a	Churn
0.008	0.043	0.063	2.4	9265	0.128	0.0261	0.0228	-81	Slug-bubbly
0.015	0.043	0.074	4.1	8138	0.203	0.0178	0.0142	-396	Taylor
0.050	0.043	0.119	8.7	6456	0.417	0.0137	0.0080	212	Taylor
0.100	0.043	0.173	5.4	4033	0.578	0.0321	0.0136	-490	Taylor
0.201	0.043	0.314	4.5	n/a	0.641	0.0704	0.0252	n/a	Taylor
0.384	0.043	0.616	3.5	n/a	0.624	0.1773	0.0667	n/a	Taylor
0.008	0.145	0.173	3.5	11081	0.047	0.0490	0.0467	867	Bubbly
0.008	0.145	0.181	3.6	n/a	0.046	0.0508	0.0485	n/a	Bubbly
0.015	0.145	0.200	5.4	10712	0.074	0.0368	0.0341	795	Bubbly
0.049	0.145	0.248	11.6	9381	0.199	0.0213	0.0170	799	Taylor
0.099	0.145	0.306	11.1	8329	0.324	0.0276	0.0186	1085	Taylor
0.199	0.145	0.433	n/a	6742	0.460	n/a	n/a	956	Slug-bubbly
0.382	0.145	0.743	7.2	5582	0.514	0.1035	0.0503	379	Churn
0.008	0.247	0.312	n/a	12077	0.026	n/a	n/a	1641	Bubbly
0.015	0.247	0.336	n/a	11938	0.044	n/a	n/a	1698	Bubbly
0.049	0.247	0.371	12.4	11148	0.132	0.0300	0.0260	1852	Slug-bubbly
0.099	0.247	0.462	n/a	10297	0.213	n/a	n/a	1871	Slug-bubbly
0.198	0.247	0.582	n/a	9502	0.340	n/a	n/a	2430	Slug-bubbly
0.380	0.247	0.848	n/a	9159	0.449	n/a	n/a	3254	Churn
0.008	0.346	0.433	n/a	12811	0.019	n/a	n/a	2298	Bubbly
0.015	0.346	0.468	n/a	12812	0.032	n/a	n/a	2438	Bubbly
0.049	0.346	0.529	n/a	12468	0.093	n/a	n/a	2748	Slug-bubbly
0.098	0.346	0.596	n/a	11953	0.165	n/a	n/a	3010	Slug-bubbly
0.198	0.346	0.717	n/a	10056	0.276	n/a	n/a	2296	Slug-bubbly
0.379	0.346	n/a	n/a	11263	n/a	n/a	n/a	n/a	Churn

Campaign 10 (3.02 mm circular capillary; air-oil system)

U_G /[m/s]	U_L /[m/s]	V_b /[m/s]	f_b /[s^{-1}]	ΔP_T /[Pa]	ε_G /[-]	L_{UC} /[m]	L_{slug} /[m]	ΔP_f /[Pa]	Flow regime
0.010	0.000	0.012	0.1	247	0.814	0.1010	0.0188	-1904	Taylor
0.018	0.000	0.024	0.4	562	0.742	0.0638	0.0165	-2417	Taylor
0.059	0.000	0.084	1.3	763	0.701	0.0651	0.0194	-2681	Taylor
0.118	0.000	0.165	2.5	640	0.717	0.0665	0.0188	-2626	Taylor
0.235	0.000	0.339	4.8	826	0.692	0.0703	0.0216	-2723	Taylor
0.339	0.000	0.514	4.5	1058	0.661	0.1130	0.0383	-2853	Taylor
0.446	0.000	0.721	n/a	1333	0.619	n/a	n/a	-3067	Churn
0.010	0.002	0.014	0.5	1570	0.718	0.0266	0.0075	-1687	Taylor
0.010	0.008	0.024	1.5	5938	0.403	0.0159	0.0095	-952	Taylor
0.018	0.008	0.035	2.3	4779	0.506	0.0149	0.0074	-922	Taylor
0.018	0.008	0.035	2.0	4618	0.505	0.0178	0.0088	-1093	Taylor
0.059	0.008	0.095	4.1	2731	0.616	0.0231	0.0089	-1696	Taylor
0.059	0.008	0.097	4.4	3071	0.605	0.0221	0.0087	-1483	Taylor
0.118	0.008	0.167	7.1	2731	0.707	0.0235	0.0069	-655	Taylor
0.234	0.008	0.355	10.3	2608	0.660	0.0345	0.0117	-1314	Taylor
0.445	0.008	0.745	2.9	2274	0.598	0.2566	0.1032	-2365	Taylor
0.641	0.008	1.165	n/a	2143	0.550	n/a	n/a	-3046	Churn
0.009	0.027	0.041	2.7	9698	0.232	0.0149	0.0115	841	Taylor
0.017	0.027	0.058	3.4	10463	0.300	0.0174	0.0122	2386	Taylor
0.058	0.027	0.123	10.0	6699	0.474	0.0123	0.0065	634	Taylor
0.117	0.027	0.212	17.0	6122	0.551	0.0125	0.0056	941	Taylor
0.234	0.027	0.376	27.5	6179	0.623	0.0137	0.0051	1835	Taylor
0.445	0.027	0.797	5.4	4473	0.558	0.1488	0.0658	-627	Taylor
0.009	0.044	0.070	3.9	12884	0.134	0.0182	0.0158	2894	Taylor
0.017	0.044	0.086	6.2	11628	0.203	0.0138	0.0110	2430	Taylor
0.058	0.044	0.152	14.0	9793	0.381	0.0108	0.0067	2653	Taylor
0.117	0.044	0.234	23.6	9053	0.498	0.0099	0.0050	3260	Taylor
0.233	0.044	0.409	34.3	8792	0.570	0.0119	0.0051	3833	Taylor
0.445	0.044	0.797	8.8	6531	0.558	0.0911	0.0403	1430	Taylor
0.642	0.044	1.109	9.0	5700	0.579	0.1235	0.0520	847	Taylor
0.009	0.078	0.119	5.9	16208	0.079	0.0202	0.0186	5579	Bubbly
0.009	0.104	0.159	7.2	18098	0.059	0.0221	0.0208	7242	Bubbly
0.017	0.104	0.344	24.4	17898	0.050	0.0141	0.0134	6940	Bubbly
0.057	0.104	0.248	31.1	17684	0.231	0.0080	0.0061	8808	Bubbly
0.116	0.104	0.320	50.0	17778	0.362	0.0064	0.0041	10415	Taylor
0.232	0.104	0.541	62.1	17154	0.428	0.0087	0.0050	10556	Taylor
0.443	0.104	0.874	21.7	12933	0.507	0.0403	0.0198	7248	Taylor

Campaign 11 (2.89 mm square capillary; air-oil system)

U_G /[m/s]	U_L /[m/s]	V_b /[m/s]	f_b /[s^{-1}]	ΔP_T /[Pa]	ε_G /[-]	L_{UC} /[m]	L_{slug} /[m]	ΔP_f /[Pa]	Flow regime
0.008	0.000	0.012	0.4	1583	0.714	0.0320	0.0092	-1718	Taylor
0.008	0.000	0.011	0.3	1823	0.758	0.0321	0.0078	-972	Taylor
0.015	0.000	0.021	0.5	1330	0.726	0.0393	0.0108	-1826	Taylor
0.051	0.000	0.074	1.5	1343	0.680	0.0509	0.0163	-2344	Taylor
0.051	0.000	0.073	1.5	1343	0.694	0.0499	0.0153	-2184	Taylor
0.101	0.000	0.146	3.5	1218	0.694	0.0420	0.0128	-2311	Taylor
0.201	0.000	0.303	6.8	1399	0.664	0.0444	0.0150	-2483	Taylor
0.291	0.000	0.459	10.3	1916	0.633	0.0444	0.0163	-2319	Taylor
0.008	0.007	0.020	1.5	6860	0.406	0.0139	0.0083	4	Taylor
0.015	0.007	0.030	2.1	5164	0.502	0.0142	0.0071	-583	Taylor
0.050	0.007	0.083	4.5	3361	0.609	0.0184	0.0072	-1154	Taylor
0.201	0.007	0.303	13.8	2980	0.664	0.0220	0.0074	-900	Taylor
0.008	0.023	0.043	3.0	10999	0.190	0.0143	0.0116	1655	Bubbly
0.015	0.023	0.053	4.3	9398	0.282	0.0124	0.0089	1110	Taylor
0.050	0.023	0.108	10.2	6931	0.463	0.0106	0.0057	731	Taylor
0.200	0.023	0.334	27.3	6189	0.599	0.0123	0.0049	1568	Taylor
0.008	0.037	0.064	3.7	12414	0.126	0.0173	0.0151	2333	Bubbly
0.015	0.037	0.077	6.1	11702	0.195	0.0124	0.0100	2420	Taylor
0.050	0.037	0.133	14.2	9745	0.375	0.0094	0.0059	2534	Taylor
0.200	0.037	0.367	35.2	8250	0.545	0.0104	0.0047	3000	Taylor
0.008	0.089	0.165	7.3	16609	0.049	0.0227	0.0216	5637	Taylor
0.015	0.089	0.168	12.8	16574	0.088	0.0132	0.0120	6057	Bubbly
0.049	0.089	0.213	32.9	16022	0.232	0.0065	0.0050	7158	Bubbly
0.199	0.089	0.446	63.8	15581	0.446	0.0070	0.0039	9188	Taylor

APPENDIX II: Discussion on the Bubble Rise Velocity

Figure 1 below shows a unit cell consisting of a pair of bubbles and a liquid slug sandwiched between them.

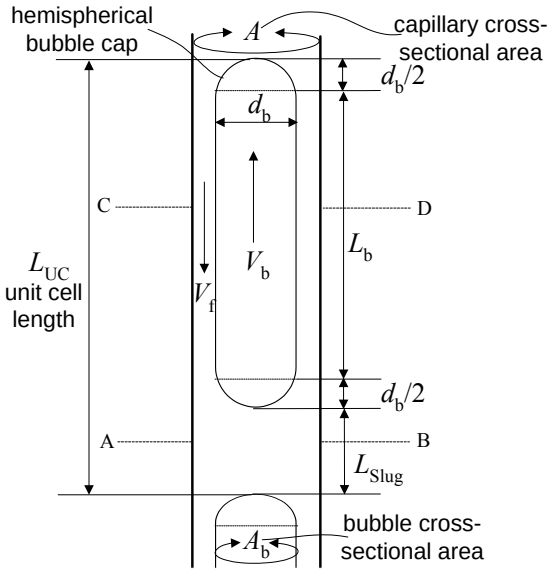

Figure 1. Representation of a unit cell

For a fully developed steady slug flow, a mass balance over half of the unit cell (indicated by ABCD) as shown in Figure 1 relative to a reference system moving with the bubble velocity yields:

$$\varepsilon_{Lf}\left(V_b - V_f\right) = V_b - U_{TP} \tag{1}$$

As seen from eq 1, the bubble rise velocity, V_b can be predicted if the liquid film velocity, V_f and the film liquid holdup, ε_{Lf} are known. Additional assumptions to eq 1 are: (1) the velocity of the liquid slug is equal to the two-phase superficial velocity, U_{TP} (2) the film flow is fully developed and (3) the effect of capillary configuration is negligibly small. Based on similar assumptions, Thulasidas et al.[1] derived the following relation for the average liquid velocity in the film of a circular capillary

$$V_f = \frac{\rho_L g d_c^2}{32\mu_L\left(1-\left(\frac{d_b}{d_c}\right)^2\right)}\left(1+4\left(\frac{d_b}{d_c}\right)^4\left(\frac{3}{4}-\ln\frac{d_b}{d_c}-\left(\frac{d_b}{d_c}\right)^{-2}\right)\right) \tag{2}$$

eq 2 is the analytical form of a fully developed, gravity-driven film flow in the annulus of a round tube. d_b and d_c are the bubble and capillary diameters respectively. The average liquid holdup in the film is related to the bubble diameter via the relationship

$$\varepsilon_{Lf} = 1 - \left(\frac{d_b}{d_c}\right)^2 \tag{3}$$

Kreutzer et al.[2] have derived a correlation for estimating the Taylor bubble diameter based on the data of Thulasidas et al.[1], which for a circular capillary is given by

$$\frac{d_b}{d_c} = 0.64 + 0.36\exp\left(-2.13Ca^{0.52}\right) \tag{4}$$

In analyzing slug flows in larger diameter tubes, Barnea[3] adopted the following bubble diameter equation

$$\frac{\delta}{d_c} = 0.0682\left[\frac{\mu_L^2}{d_c^3 g(\rho_L - \rho_G)\rho_L}\right]^{1/3}\left(\frac{4\rho_L V_f \delta}{\mu_L}\right)^{2/3} \tag{5}$$

where δ is the liquid film thickness, related to the capillary diameter by

$$\frac{\delta}{d_c} = 0.5\left(1 - \frac{d_b}{d_c}\right) \tag{6}$$

The holdup of liquid in the film was estimated by

$$\varepsilon_{Lf} = 4\frac{\delta}{d_c} - 4\left(\frac{\delta}{d_c}\right)^2 \tag{7}$$

Therefore, V_f and ε_{Lf} can be estimated separately from these two independent studies: (1) Using eqs 2, 3 and 4. (2) Using eqs 4, 5, 6 and 7. We refer to the first and second methods as Methods 1 and 2 respectively. Figure 2a shows the parity plot for the experimental and predicted bubble rise velocities obtained using both methods. We however developed a simple approach of estimating the bubble rise velocity that eliminates the need to estimate the bubble diameter or liquid film flow rate given by the relationship

$$\frac{V_b}{U_{TP}} = \frac{1}{1 - 0.61Ca^{0.33}} \tag{8}$$

The parity plot based on the use of eq 8 is shown in Figure 2b, referred to as Method 3. A very good agreement is also achieved.

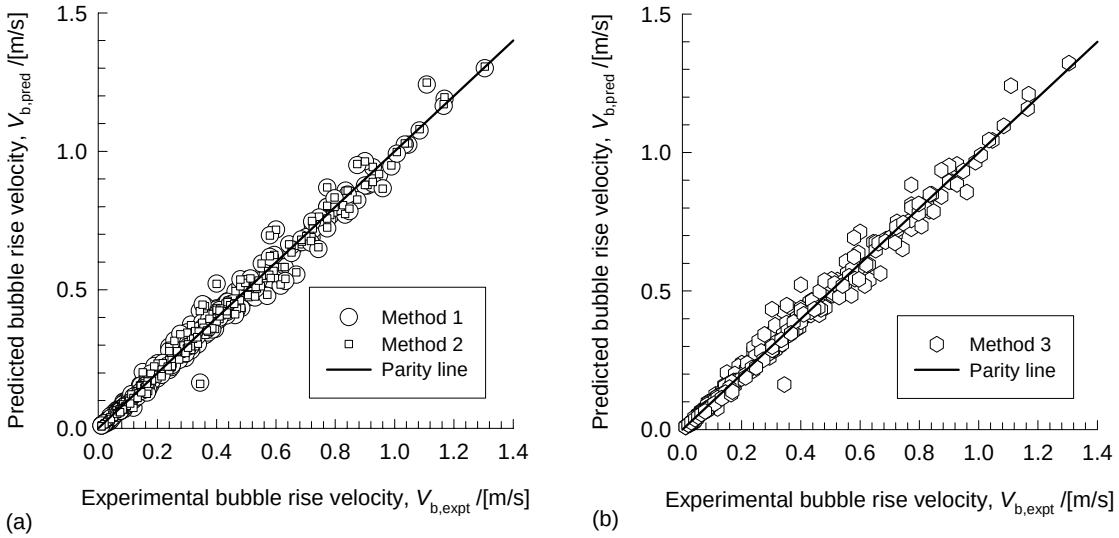

Figure 2. (a) Comparison of the experimentally observed and predicted bubble rise velocities using Methods 1 and 2 (b). Comparison of the experimentally observed and predicted bubble rise velocities using Method 3.

Notation

d_b	Taylor bubble diameter, m
d_c	capillary hydraulic diameter, m
f_b	bubble frequency, s^{-1}
g	gravitational constant, m/s^2
L_{slug}	liquid slug length, m
L_{UC}	unit cell length, m
P_f	frictional pressure, Pa
P_T	total pressure, Pa
U_G	superficial gas velocity, m/s
U_L	superficial liquid velocity, m/s
U_{TP}	two-phase superficial velocity (U_G+U_L), m/s
V_b	bubble rise velocity, m/s

V_f liquid film velocity, m/s

Greek symbols

δ liquid film thickness, m

ε_G gas holdup, dimensionless

ε_{Lf} film liquid holdup, dimensionless

μ_L liquid viscosity, Pa s

ρ_G gas density, kg/m^3

ρ_L liquid density, kg/m^3

Dimensionless groups

Ca capillary number ($\mu_L U_{TP}/\sigma$)

Subscripts

expt refers to experimental data

pred refers to model or correlation predicted data

Literature cited

(1) Thulasidas, T. C.; Abraham, M. A.; Cerro, R. L. Bubble-Train Flow in Capillaries of Circular and Square Cross- Section. *Chem. Eng. Sci.* **1995**, *50*, 183-199.

(2) Kreutzer, M. T.; Du, P.; Heiszwolf, J. J.; Kapteijn, F.; Moulijn, J. A. Mass transfer characteristics of three-phase monolith reactors. *Chem. Eng. Sci.* **2001**, *56*, 6015-6023.

(3) Barnea, D. Effect of bubble shape on pressure drop calculations in vertical slug flow. *Int. J. Multiphase Flow* **1990**, *16*, 79-89.